Topical delivery of human single-domain antibody targeting IL-33 for inhibiting mucosal inflammation

Tianlei Ying

tlying@fudan.edu.cn

Fudan University https://orcid.org/0000-0002-9597-2843

Keke Huang

MOE/NHC/CAMS Key Laboratory of Medical Molecular Virology, Shanghai Frontiers Science Center of Pathogenic Microorganisms and Infection, Shanghai Institute of Infectious Disease and Biosecurity, Sch

Yuqing Wu

Department of Ophthalmology and Vision Science, Eye, Ear, Nose and Throat Hospital, Fudan University

Yu Kong

MOE/NHC/CAMS Key Laboratory of Medical Molecular Virology, Shanghai Frontiers Science Center of Pathogenic Microorganisms and Infection, Shanghai Institute of Infectious Disease and Biosecurity, Sch

Qingyuan Xu

Department of Pulmonary Medicine, Zhongshan Hospital, Fudan University

Yirou Zhang

Department of Ophthalmology and Vision Science, Eye, Ear, Nose and Throat Hospital, Fudan University

Quanxiao Li

MOE/NHC/CAMS Key Laboratory of Medical Molecular Virology, Shanghai Frontiers Science Center of Pathogenic Microorganisms and Infection, Shanghai Institute of Infectious Disease and Biosecurity, Sch

Cheng Li

MOE/NHC/CAMS Key Laboratory of Medical Molecular Virology, Shanghai Frontiers Science Center of Pathogenic Microorganisms and Infection, Shanghai Institute of Infectious Disease and Biosecurity, Sch

Wenping Song

MOE/NHC/CAMS Key Laboratory of Medical Molecular Virology, Shanghai Frontiers Science Center of Pathogenic Microorganisms and Infection, Shanghai Institute of Infectious Disease and Biosecurity, Sch

Xiaoyi Zhu

MOE/NHC/CAMS Key Laboratory of Medical Molecular Virology, Shanghai Frontiers Science Center of Pathogenic Microorganisms and Infection, Shanghai Institute of Infectious Disease and Biosecurity, Sch

Zhenlin Yang

Department of Pulmonary Medicine, Zhongshan Hospital, Fudan University

Changchang Xin

Department of Ophthalmology and Vision Science, Eye, Ear, Nose and Throat Hospital, Fudan University

Xujiao Zhou

Department of Ophthalmology and Vision Science, Eye, Ear, Nose and Throat Hospital, Fudan University

Yanling Wu

Key Laboratory of Medical Molecular Virology (MOE/NHC/CAMS), School of Basic Medical Sciences and Shanghai Public Health Clinical Center, Fudan University

Jiaxu Hong

Department of Ophthalmology and Vision Science, Eye, Ear, Nose and Throat Hospital, Fudan University

---

Article

Keywords:

Posted Date: September 30th, 2024

DOI: https://doi.org/10.21203/rs.3.rs-4975440/v1

Additional Declarations: (Not answered)

Abstract

Addressing mucosal inflammatory disorders in the ocular surface or respiratory system remains a formidable challenge due to limited penetration of biological therapeutics across epithelial barriers. In this study, we explored the potential of human single-domain antibodies (UdAbs) as topical therapeutics for the targeted modulation of interleukin-33 (IL-33) in two mucosal-associated inflammatory disorders. The anti-IL-33 UdAb, designated A12, demonstrated potent inhibition of the IL-33-mediated signaling pathway, despite not blocking IL-33 receptor interaction. The topical delivery of A12 achieved significantly elevated corneal concentrations *in vivo* compared to anti-IL-33 control IgG Itepekimab, which exhibited negligible ocular penetration. Meanwhile, A12 ameliorated the dry eye disease severity considerably by exerting anti-inflammatory effects. Furthermore, in another murine model of allergic asthma, inhaled A12 substantially reduced overall lung inflammation. Our findings revealed the capacity of UdAbs to penetrate mucosal barriers following non-invasive localized delivery, highlighting their potential as an innovative therapeutic strategy for modulating mucosal inflammation.

Introduction

Inflammatory disorders, such as dry eye disease or allergic asthma, significantly impact quality of life and contribute to increased mortality (1). These disorders are characterized by aberrant inflammatory responses localized to mucosal epithelia, including the ocular surface and pulmonary airways. To date, a number of therapeutic antibodies targeting inflammation-related targets have been widely developed for the treatment diseases like neovascular age-related macular degeneration and severe asthma (2, 3). However, the impermeable nature of mucosal barriers limits penetration of systemically administered antibodies. For example, less than 2% of intravenously injected antibodies reach ocular tissues due to the outer blood–retinal barrier of retinal pigment epithelium (RPE) with tight junctions (4). Similarly, previous pharmacokinetics studies in primates showed that only ~ 0.2% of systemically administered antibodies could be recovered in the bronchoalveolar lavage (BAL) fluid (5). The poor bioavailability at inflamed mucosal sites leads to suboptimal therapeutic effects and often necessitates high systemic doses, increasing risks of adverse effects (6). In recent years, a variety of non-systemic approaches, such as local injection of therapeutic antibodies for improving local concentration, have been implied in ocular diseases (7). Nonetheless, it requires specialized personnel for administration, posing a tremendous burden on the individual and the health-care system and poor patient compliance. Furthermore, the invasive nature of local injection can result in trauma and high risk of infection. Therefore, there has been significant interest in developing a more tolerable therapeutic strategy for long-term treatment regimens.

Topical delivery is the most common and convenient way which can avoid above-mentioned complications and efficiently target mucosal inflammatory disorders. However, rare studies have reported the use of topical delivery platforms for therapeutic antibodies. Firstly, their large molecular weight and poor tissue penetration would decrease the delivery efficiency and affect drug distribution. Additionally, antibodies are susceptible to denaturation and aggregation when formulated for localized

delivery or under extra-pressure, which may not only lead to loss of activity but also improved immunogenicity. While topically delivered bevacizumab with cell-penetrating peptides could deliver antibody to the posterior segment and showed therapeutic effect in a model of choroidal neovascularization (CNV) (8), concerns remain regarding the stability and immunogenicity of such complexes that may hinder further development. Various kinds of engineered antibody fragments with smaller size, such as Licaminlimab, a single-chain antibody fragment (scFv) that binds to TNF-α, have been developed. Topical ocular administration of Licaminlimab relieved ocular discomfort in patients with severe dry eye disease (DED) (9). However, stability and immunogenicity concerns still exist due to the susceptibility of fragments to aggregation and denaturation.

Single-domain antibodies (sdAbs), an alternative novel antibody format that derived from the VH domain of camelid heavy-chain-only immunoglobulins, as known nanobodies, are frequently exploited to disease therapy (10). Common to all sdAbs is that they are small (12–15 kDa), retain strong affinity for binding to antigen, and possess high stability (11). Combined, this enables them to withstand high temperature and pressure, extreme pH, and proteolysis, and maintain functionality, which lends them particularly well to topical delivery. Nevertheless, the animal origin of nanobodies raises safety concerns related to immunogenicity caused by the non-human sequences, resulting in their limited applications in clinic. Our group previously developed human single-domain antibody (UdAb) library by grafting human naive complementarity-determining regions (CDR) into framework regions of a heavy chain variable region allele (12). We demonstrated that high-affinity UdAbs targeting various targets possess high stability and can be delivered through inhalation (13, 14). As a proof of concept, one bispecific antibody integrating two UdAbs recognizing different epitopes has completed phase II clinical trial, indicating good tolerability and safety [CXSL2300258].

It is known that type 2 cytokines are crucial to the pathogenesis of many inflammatory diseases (15). One of predominantly epithelial cell–derived cytokine, interleukin-33 (IL-33), has emerged as important initiators of mucosal inflammation. IL-33 belongs to the IL-1 family (16) and is widely expressed in the mucosal endothelial cells (17, 18). When cells are damaged or stressed by allergens or pathogens, IL-33 as a key alarm cytokine is released from the epithelium and other local stromal compartments and activates signaling pathway mediated by IL-33-ST2 axis, thereby triggers the innate and adaptive immune systems (19). Recent studies have revealed IL-33 aberrational elevation propagating mucosal inflammation in diseases like asthma (20), atopic dermatitis (21), rheumatoid arthritis (22), chronic obstructive pulmonary disease (COPD) (23), and dry eye diseases (24). Indeed, neutralizing IL-33 by monoclonal antibodies showed efficacy in dampening mucosal inflammation in animal models (25, 26). However, in a clinical study for treatment patients with moderate-to-severe asthma using Itepekimab (REGN3500), a monoclonal antibody targeting IL-33, showed inferior therapeutic efficacy compared to approved therapeutics via subcutaneous administration (27), suggesting low effectiveness of systemic antibody delivery for mucosal inflammation treatment. Therefore, in this study, we aimed to investigate the potential of UdAbs as topical therapeutics for treatment of inflammatory diseases. For this purpose, we developed a UdAb targeting IL-33, named as A12, which exhibited superior structural integrity and high-affinity antigen binding (3.23 nM). Although UdAb A12 did not block IL-33 interaction with its

receptor ST2, it potently inhibited IL-33 signaling pathway *in vitro*. We utilized two models, dry eye disease (DED) and allergic asthma, to investigate the therapeutic efficacy of the topical delivered A12. In a murine DED model, topical ocular instillation of UdAb A12 demonstrated superior anti-inflammatory efficacy *in vivo* as assessed by disease scoring. Furthermore, in an ovalbumin-induced allergic asthma model, inhalation of UdAb A12 markedly reduced IgE levels, lung eosinophilia, and lung inflammation. These findings highlight therapeutic potential of UdAbs as topical biologics for localized treatment of mucosal inflammatory disorders.

Results

UdAb A12 inhibits IL-33-induced signaling pathway by targeting a non-blockade epitope for its receptor interaction

The full-length human IL-33 protein is composed of two evolutionarily conserved domains, N-terminal nuclear domain (amino acids 1–65) for nuclear localization and C-terminal IL-1-like cytokine domain (amino acids 112–270) that is responsible for IL-33/ST2 complex conformation and confers the cytokine-like activities (28). Therefore, the coding sequences of C-terminal domain including amino acids 112–270 were synthesized and cloned into an expression vector. After expression and purification, the IL-33 protein was biotinylated and used as antigen for antibody panning from naïve phage library displaying UdAb (Fig. 1A) (12). Binding to IL-33 was enriched during four rounds of selection and eight of unique UdAbs were identified. These UdAbs were expressed in *Escherichia coli* and characterized for their biophysical properties, including yield, purity, aggregation and thermal stability. Among these, A12 demonstrated a single peak in size-exclusion chromatography (SEC) and dynamic light scattering (DLS), whereas most UdAbs tended to aggregate and form large particles (**Figure S1**). Hydrophobic interaction chromatography (HIC) results also indicated that the antibody A12 exhibits hydrophilicity comparable to that of the marketed monoclonal antibodies Keytruda and Herceptin (**Figure S1D**). Notably, the UdAb A12 exhibited the most advantageous properties among all tested antibodies, and had a binding affinity of 3.23 nM (k_{on} = 1.13×10^4 M^{-1} s^{-1}, k_{off} = 5.66×10^{-3} s^{-1}) as measured by bio-layer interferometry (Fig. 1B).

IL-33 signals to cells through the membrane-bound receptor ST2 (29). As such, we investigated whether A12 confers impact on the interaction between IL-33 and ST2 using competitive binding assays. We found that IL-33 maintained binding activity to ST2 in the presence of A12 (Fig. 1C, S2A-B), indicating it likely binds a non-overlapping epitope. Similarly, the IL-33 neutralizing antibody Itepekimab, a type of human IgG4 antibody developed by Regeneron Inc. and was in phase II (27), did not compete with ST2 (Fig. 1C, S2C). However, competitive binding studies revealed A12 and Itepekimab do not share an overlapping epitope on IL-33 either (Fig. 1C, S2D), indicating A12 recognizes a novel epitope on IL-33.

Studies have revealed that binding of ST2 allows IL-33 to interact with IL-1RacP, an IL-1 super-family member co-receptor, and this IL-33 receptor complex signals through MyD88, IRAK1, and IRAK4 kinases and TRAF6 to culminate in the activation of several MAP kinases and NF-κB (16, 30). Therefore, we next

tested whether A12 impacted formation of the IL-33/ST2/IL-1RacP ternary signaling complex. Interestingly, A12 could inhibit recruitment of IL-1RacP co-receptor to the IL-33/ST2 binary complex, similar to Itepekimab (Fig. 1C, S2E-G).

To further elucidate the impact of A12 on IL-33 signaling, we utilized HUVEC cell line expressing the IL-33 receptor ST2 and co-receptor IL-1RacP to assess effects on the NF-κB pathway. We first confirmed IL-33 could activate NF-κB signaling by inducing nuclear translocation of NF-κB (Fig. 1D). Next, prior pre-incubation with IL-33 and A12 or control antibody at a concentration of 10 μg/mL, the mixture was added into HUVEC cells and NF-κB activation signaling was measured. We observed that A12 markedly suppressed IL-33-induced NF-κB activation (Fig. 1D), indicating A12 can potently inhibit IL-33 downstream signaling. In summary, although A12 does not directly block IL-33 binding to ST2, it can effectively inhibit IL-33-mediated signal transduction through interfering with IL-1RacP co-receptor recruitment and attenuating NF-κB activation.

Blockade of IL-33 exhibits anti-inflammatory effect in vitro

Recently, emerging studies indicate that IL-33/ST2 axis is also involved in pathogenesis of a wide range of ocular diseases, such as dry eye disease (DED) (17). To evaluate the potential efficacy of blocking IL-33 activity via A12, we employed a hyperosmotic stress-induced human ocular epithelial cells (HCECs) model of DED. HCECs represent the frontline of innate ocular immunity (31). When HCECs exposed to 500 mOsm of hyperosmolarity stress, we characterized inflammatory cytokine expression kinetics in HCECs. Consistent with previous studies (32), we observed that hyperosmotic stress significantly increased *Il-33* expression, as well as other pro-inflammatory cytokines mRNA including *Il-6, Il1-b* and *Tnf-a* (Fig. 2A). Interestingly, the peak of *Il-33* mRNA expression occurred at 15 minutes post-hyperosmotic stress insult, returning to normal levels by 24 hours. In contrast, *Il-6* and *Tnf-a* exhibited their mRNA expression peaks at 30 minutes, while *Il1-b* peaked at 4 hours post-stress, and maintained their increased expression at 24 hours (Fig. 2A). The temporal pattern underscores the alarming role of IL-33. Since IL-33 expression level peaked at 15 minutes post-stress, we firstly utilized this timepoint to investigate the inhibitory activity of A12. Indeed, compared to normal osmotic conditions, hyperosmotic stress dramatically increased IL-33 concentration in supernatants and *Il-33* mRNA expression in HCECs (Fig. 2B and 2C). In contrast, A12 treatment led to a dose-dependent reduction in IL-33, with 2 μg/mL A12 decreasing IL-33 to 25.95 pg/mL (Fig. 2B). Further assessment revealed 2 μg/mL A12 significantly downregulated hyperosmotic stress-induced *Il-33, Il-6*, *Tnf-a* and *Il1-b* mRNA expression ($p < 0.01$, $p < 0.05$, $p < 0.001$, $p < 0.05$ respectively) (Fig. 2C). Furthermore, at 24 hours post-stress, IL-33 concentration in supernatants increased to 96.16 pg/mL, compared to 58.97 pg/mL (Fig. 2D). Upon A12 treatment, the mRNA of *Il-33* promptly decreased, simultaneously suppressing mRNA expression of *Il-6*, *Tnf-a* and *Il1-b* (Fig. 2E). Correspondingly, cell viability assays also showed decreased viability of 56.3% after hyperosmotic stimulation, while A12 with 2 μg/mL significantly improved cell viability ($p < 0.0001$, Fig. 2F). Compared to the Itepekimab, an anti-IL-33 monoclonal antibody in an IgG format, A12 demonstrated comparable anti-inflammatory effects and cell viability enhancement at the same

concentration **(Figure S3)**. Together, these *in vitro* results demonstrated potent anti-inflammatory effects of A12 in DED models, supporting further investigation of its therapeutic potential *in vivo*.

Topical instillation as an effective route for delivery of A12 to the eye

Topical instillation is the predominant clinical route for drug administration to treat dry eye disease (33). However, challenges including large size, poor tissue permeation, and low stability of proteins impede their efficacy via topical instillation (33). Leveraging the favorable size and stability properties of human single-domain antibodies, we explored the potential of topical delivering human single-domain antibodies for corneal penetration.

To compare the performance of A12 with the conventional IgG antibody for ocular penetration in mice, we first conjugated the antibodies with DyLight 650 to enable imaging. We employed the freshly enucleated eyeball of wild type C57BL/6 mice as *ex vivo* model. To mimic disrupted corneal epithelium barrier in dry eye disease, 0.1% benzalkonium chloride was added according to previous study (34) **(**Fig. 3A**)**. After 12 hours of antibody incubation, imaging indicated a greater corneal penetration of A12 compared to Itepekimab, with a 3-fold higher fluorescent intensity (Fig. 3B and 3C). To further assess *in vivo* distribution, C57BL/6 mice were treated with antibody through topical instillation and measured the fluorescence in eyeballs at various timepoints (**Figure S4A).** *In vivo* bio-imaging also indicated A12 had a significant presence in the cornea, with highest fluorescence detectable at 15 minutes post-instillation (**Figure S4B and S4C**). Additionally, A12 exhibited distribution in the conjunctiva (**Figure S4D**). In contrast, Itepekimab showed few in the cornea and no accessible to the conjunctiva. Neither A12 nor Itepekimab reached the retina (Fig. 3E, **Figure S4E**). Therefore, we further quantified the antibody concentrations in eyeballs at various timepoints (Fig. 3D). The results revealed A12 effectively penetrated ocular tissues, reaching peak concentrations at 1.3 hours, whereas Itepekimab showed no detectable in ocular tissues **(**Fig. 3E**)**. The amount of A12 penetration was over 20-fold higher than Itepekimab **(**Fig. 3F**)**. Together, these results indicated that A12 has superior permeability across the ocular surface barrier compared to conventional IgG antibodies.

The potential effects of A12 as topical eye drop in a DED mice model

To investigate the anti-inflammatory therapeutic effect of A12, a DED mouse model was induced by subjecting mice to 14 days of low humidity (relative humidity < 20%) in a controlled environment chamber (CEC) (35). We explored whether A12 binds to mouse IL-33 and performed sequence alignments of IL-33 protein between human and mouse. Numerous differences were observed, and the homology was found to be only 55% (16)(**Figure S5A**). ELISA results also indicated that A12 specifically binds to human IL-33 (**Figure S5B**). Therefore, C57BL/6 mice with genetically engineered human IL-33 was employed. Following desiccation, mice were randomly assigned to receive either PBS or A12 (60 μg/μL) three times daily for 7 consecutive days, with observations conducted at day 14 (Fig. 4A). Positive

fluorescein staining spots on day 0 in DED mice, compared to the control, confirming the successful establishment of the dry eye model (Fig. 4B). In the DED group, a modest decline in the corneal fluorescein score (CFS) was noted on day 7, followed by a resurgence after discontinuation of PBS on day 14. Conversely, after a 3-day A12 treatment, corneal fluorescence rapidly decreased, gradually diminishing until day 7, and maintained a lower score even after A12 withdraw on day 14. Notably, CFS scores in A12-treated eyes were significantly lower at different observation time points compared to the DED group (14.25 vs 8.38 on day 3, $p < 0.0001$; 12.50 vs 5.00 on day 5, $p < 0.001$; 10.75 vs 3.88 on day 7, $p < 0.0001$; 10.88 vs 3.75 on day 14, $p < 0.0001$; Fig. 4B and 4C). Tear production remained similar between the two groups during the observation period (**Figure S6A**). Histomorphology assessments were then conducted to investigate structural and morphological changes in the ocular surface after treatments. Hematoxylin & Eosin (H&E) staining displayed a thinning of the corneal superficial epithelial layers after DED modeling in DED group (26.49 μm ± 0.33 μm), while the A12 group showed a recovery of corneal epithelial thickness (33.20 μm ± 1.72 μm) similar to that of the control group (30.99 μm ± 1.16 μm) (Fig. 4D and 4E). The mucus layer, the innermost layers of tear film responsible for lubrication in ocular surface and tear film homeostasis, was assessed using periodic acid-Schiff (PAS) staining. In DED group, the conjunctival fornix was nearly deprived of goblet cells, whereas A12 treatment markedly restored goblet cell density to levels comparable to the control group (Fig. 4D and 4F). Consistent with PAS staining, immunofluorescence staining of mucin 5AC (Muc5AC) showed an abundantly endowment of positive-stained cells in A12 group (Fig. 4G, S6B). Quantitative real-time PCR (RT–qPCR) of corneal and conjunctival tissues demonstrated that A12 treatment in DED mice resulted in a reduction of mRNA levels of three classic inflammatory cytokines, including *Il1-b, Tnf-a, Il-6*, compared to the DED group (Fig. 4H). Furthermore, apoptotic signals were detected in both cornea and conjunctiva in DED group. In contrast, A12 treatment rescued cell apoptosis induced by desiccating stress, with few apoptotic cells in ocular surface tissues (**Figure S7**). These findings indicate the superior therapeutic effect of A12 in restoring corneal structure, maintaining mucin content in the conjunctiva, reducing inflammatory cytokines, and rescuing cell apoptosis.

Encouraged by the inspiring therapeutic efficacy of phenotype, we further explored the potential mechanism of A12 behind the alleviation of dry eye syndrome. The gene expression levels of A12 targets, *mST2*, was upregulated on ocular surface in the DED group, while it was downregulated in A12 group (Fig. 4I). However, the gene expression of *hIL-33* was unchanged in all groups, which may explain by the function of alarmin of IL-33 (Fig. 4I). Compared with RT–qPCR results, immunofluorescence staining revealed a noticeably positive expression of hIL-33 and mST2 protein in conjunctiva stroma (Fig. 4J, S6C-D). The ocular surface immunoregulation relies significantly on the integrity of corneal epithelium and goblet cells (36). In DED, extrinsic insults and inflammatory cytokines disrupt the ocular surface, abrogating immune tolerance and promoting resident antigen-presenting cells (APC) to adopt “mature” phenotypes (37). These phenotypes are characterized by an upregulated expression of MHC class II (MHC-II) and co-stimulatory molecules B7 (CD80 and CD86) (37–39). Herein, we performed immunofluorescence staining for mature macrophage marker F4/80 in the ocular surfaces of all group. We found increased frequencies of $F4/80^+$ cells within the ocular surface in DED mice treated with PBS

compared to naïve mice, whereas treatment with A12 decreased the frequencies of F4/80$^+$ cells (Fig. 4K). In DED, activated antigen-bearing APCs migrated from ocular surface to draining lymph node (DLN), where mature APCs can induce naïve CD4$^+$ T cells to differentiate into different effector T cells (40). We next investigated whether A12 treatment downregulated the APC trafficking to DLNs and the priming of T cells. Flow cytometric analysis of DLNs showed a remarkable increased frequencies of mature APCs (CD11c$^+$ MHCII$^+$) and macrophages (CD11c$^+$ F4/80$^+$) in DED group compared to naive mice, while treatment with A12 significantly decreased these frequencies (Fig. 4L). Moreover, we confirmed that the population of IFN-γ expressing CD4$^+$ T cells as also notably increased in DED group, whereas a depletion of Th1 cells was found in A12 group (Fig. 4M). Additionally, A12 treatment also reduced the frequency of ST2$^+$ CD4$^+$ T cells in DED mice DLNs, but a surprising upregulation of these cells was found in DED group (Fig. 4N). Given the prominent therapeutic results, *ex vivo* biosafety experiment of A12 in human corneoscleral rim were carried out. TUNEL assay was used to evaluate cell apoptosis. As is shown in **Figures S8**, fluorescein staining showed no distinct TUNEL signal in A12 (10 mg/mL, 60 mg/mL and 100 mg/mL) treated group.

All in all, we demonstrated that human single-domain antibody A12 could be efficiently delivered to ocular surface via topical instillation, exert excellent anti-inflammatory profile in DED and hold great potential for future clinical application.

The potential effects of A12 through inhalation in an asthma mice model

With evidence indicating the significant impact of A12 in alleviating inflammation through blockade of IL-33 signaling, we explored the potential of this unique domain antibody to ameliorate inflammatory pathology in a distinct disease model. Our focus turned to asthma, a complex condition influenced by genetic susceptibility and environmental interactions, affecting approximately 334 million people worldwide (41). Asthma, an allergic disorder, characterized by elevated levels of type 2 inflammatory cytokines (IL-4, IL-5, and IL-13), increased IgE production, and eosinophils infiltration into lung tissues (21), demonstrated strong correlation with increased IL-33 levels (42).

Inhalation delivery has been an emerging route for the treatment of lung diseases. In our previous work, UdAbs could be inhaled to aerosol particles of size 3–5 μm and efficiently deposited in lung via intranasal inhalation (13). Here, we also found that A12 strongly bound to IL-33 before or after inhalation and exhibited unchanged binding activities, indicating high stability of A12 **(Figure S9)**. Moreover, we used the Next Generation Impactor (NGI) to determine the aerodynamic characteristics of A12 and IgG Itepekimab after aerosolization by using a vibrating mesh nebulizer. As expected, inhaled A12 mostly deposited on stage 5, indicating the cut-off diameter of A12 after inhalation was approximately 2.08 μm. Therefore, A12 exhibited the potential for aerosol deposition within respiratory tract. In contrast, majority of the IgG Itepekimab remains in the device under the same conditions (**Figure S10A**). To test whether aerosol particle size affects the performance of antibody in mice, we carried out a single-dose *in vivo* pharmacokinetics study of A12 and Itepekimab through inhalation route using the high-pressure

microsprayer (**Figure S10B**). After inhalation, two mice per group were euthanized for collection the lung, trachea and blood at indicated time points. The concentration of antibodies in each sample was quantified by ELISA. The results showed that the IgG Itepekimab mainly deposited in the trachea since the large size of particles that of more than 5 μm, resulting in them failed to deposit in the lung (**Figure S10C-E**) (43). Remarkedly, there are much higher concentration of A12 in lung than trachea or circulating blood, indicating the effective deposition of A12 in the lung (**Figure S10C-G**). These results indicate that A12 can be directly to lung by inhalation.

Finally, we sought to assess the *in vivo* therapeutic effects of A12 against allergic asthma. We used an Ovalbumin (OVA)-induced mouse asthma model that is characterized by eosinophilic asthma through TH2 mediated inflammatory response and widely used to verify anti-asthmatic activity of drugs (44). C57BL/6-IL-33$^{tm1(hIL-33)}$ mice were intraperitoneally sensitized with a low dose of OVA at day 0 and day 7, and challenged with a high dose of OVA on day 14–16 after inhalation administration (INH) of either PBS or A12 (Fig. 5A). Delivery of A12 targeting IL-33 in the lung robustly inhibited multiple features of OVA-induced asthma. Specifically, mice exposed to OVA showed significantly higher level of serum IgE, whereas A12 inhalation significantly reduced IgE level (Fig. 5B). Goblet cell metaplasia, a key pathologic manifestation of asthma characterized by increased production of Muc5AC, was investigated to determine whether A12 treatment could ameliorate the impaired mucociliary clearance in asthma. Strikingly, histopathologic analysis confirmed a reduction in mucus-producing cells in A12-treated mice (Fig. 5C and 5D). In paralleled with histopathologic findings, A12 inhibited lung *Muc5ac* mRNA production in OVA-induced allergic asthma (Fig. 5E**)**. Further analysis of the effect of A12 on cellular infiltration using flow cytometry demonstrated a decrease in lung eosinophilia infiltration and ratio of lung CD4$^+$/CD8$^+$ T cells after A12 treatment (Fig. 5F). Consistent with the finding of cell types, analysis of cytokine mRNA confirmed upregulation of multiple signature genes related to type 2-inflammtion (*Il-33*, *St2*, *Il-4*, *Il-5* and *Il-13*) in the lung and airway-draining lymph node exposed to OVA, whereas the expression of these cytokines was blocked in A12-treated group (Fig. 5G and 5H, S11**)**. Moreover, immunofluorescence staining of the lung revealed a reduced positive-staining of IL-33$^+$ and ST2$^+$ cells in A12 treated mice compared to OVA-exposed mice (Fig. 5I and 5J). Taken together, the current data suggested that inhalation of A12 significantly reversed pathological progress in OVA-induced asthma model.

Discussion

IL-33 is primarily known as an alarmin cytokine that triggers immune responses in mucosal inflammatory diseases, underscoring the pressing need for the development of topically applicable IL-33 specific biologics (17, 30). Here, a fully human single-domain antibody, A12, was developed, demonstrating specifical binding activity against IL-33 and the inhibition of IL-33-mediated NF-κB signaling pathway. Importantly, A12 can serve as a topical delivery biologic, either via instillation to ocular tissues or inhalation (INH) to the respiratory tract, exhibiting anti-inflammatory therapeutic efficacy in both the DED model and the asthma model.

Monoclonal antibodies (mAbs) stand out as one of the most significant categories of biologics, demonstrating their effectiveness across a diverse range of diseases, which is attributed to enhanced specificity, increased druggability, and versatile mechanism of actions (45). Since the approval of the first therapeutic antibody in 1986 (46), more than 100 antibody-based therapeutics have been approved (47). Advancement in antibody engineering and a deeper comprehension of antibodies have led to the emergence of novel antibody formats, including single-chain variable fragment antibodies (scFv), single-domain antibodies (sdAb, camel-derived also known as nanobodies), antibody-drug conjugates (ADCs) (48). Among these, sdAbs, comprising only the variable region of the heavy chain, represent the smallest antibody and can recognize some cryptic epitope, exhibiting enhanced protective efficacy (12, 13). Compared to camel-derived single-domain antibodies, our UdAbs incorporates human germline framework regions (FR1, FR2, and FR3) and human heavy-chain complementarity-determining regions (CDR1, CDR2, and CDR3). Furthermore, one bispecific antibody integrating two UdAbs has demonstrated good tolerability and safety in humans. Taken together, A12 seemed to exhibit low immunogenicity and good safety.

Despite the challenges posed by tissue barriers, topical administration of antibody-based therapeutics remains the preferred delivery route in clinical settings, due to its advantages, including better patient compliance, higher local drug concentration, and a lower risk of systemic side effects compared to systemic injection. In ocular disease, however, topical antibody delivery faces significant challenges owning to large molecular weight and tight junction in the cornea. For example, topical delivery of monoclonal IgG1, bevacizumab (150 kDa), is limited in penetrating intact cornea unless administered though subconjunctival injection (49). Recent studies highlight OCS-02, a scFv targeting TNF-α (26.7 kD), delivered as eye drops to alleviate severe DED [50]. In comparison, single-domain antibodies prove advantageous due to their stability and smaller size, facilitating easier traverse through ocular surface barriers. The instillation of A12, as demonstrated, achieves high bioavailability, and penetration experiments with fluorescence imaging also revealed a concentrated presence in the cornea epithelium.

Interestingly, the IL-33/ST2 axis is implicated in various non-allergic mucosal inflammatory disease, including dry eye disease, rheumatoid arthritis and colitis (50). The ocular mucosal system shares similarities with the airway, including the cover of mucus, presence of goblet cells and immune cells, and mucosal tolerance mechanisms (51). Dry eye disease (DED) is a multifactorial disorder of ocular surface, characterized by chronic inflammation due to a disturbance of immune homeostasis (52). In human corneal and conjunctival epithelial cells, both the RNA and protein levels of IL-33 significantly increase under hyperosmotic conditions (24, 53). Moreover, tears from patients with DED exhibit a significant elevation in IL-33 concentration, accompanied by elevated levels of various pro-inflammatory cytokines and chemokines (54). Studies have revealed that IL-33 released from corneal epithelium under environmental stress is associated with corneal defect and the amplification of inflammatory cascades in DED (55). In the DED model of ST2-deficient mice, there was a notable improvement in the integrity of the ocular surface barrier, along with improvements in other dry eye-related indicators (56). These findings demonstrate IL-33 as a promising therapeutic target in DED. The utilization of IL-33 neutralizing antibody ameliorated corneal epithelial injury (55), aligning with our own results. Moreover, our data

demonstrate that the administration of A12 alleviates ocular mucosal inflammation by downregulating proinflammatory cytokines and blocking the trafficking of APCs and Th1 cells. It's worth noting that in previous studies, mice with DED mainly received a 14-day treatment to achieve therapeutic efficiency (57). In contrast, our study reveals that a short 7-day regimen of A12 is sufficient to suppress ocular inflammation in DED, and this effect persists even after the withdraw of A12.

Additionally, previous studies have established that elevated IL-33 levels contribute to asthma exacerbation and steroid resistance (25, 58). Several IL-33-targeting biologics, including mAbs against ST2 (RG6149; CNTO7160) and mAbs binding IL-33 (ANB020; REGN3500), have been developed for asthma therapy. However, low efficacy was observed in clinical trials using systemic administration (59). Notably, a previous study demonstrated that a bispecific human single-domain antibody exhibited superior therapeutic efficacy through inhalation compared to intravenously administration for treating lung infection (13). Expanding on this, we demonstrated the efficient delivery of the single-domain antibody A12 to lung tissues via inhalation. Our results revealed that inhalation of A12 led to a noticeably reduction in various asthma-related indicators, including decreased serum IgE levels, lower eosinophil infiltration, and suppression of Th2-releated cytokines. These findings are consistent with previous studies (50), suggesting the feasibility of A12 in asthma treatment.

The therapeutic mAbs targeting IL-33 for clinical trials tends to utilize the IgG4-PAA format, where the modified Fc portion contains an S228P mutation in the hinge region to reduce half-antibody formation and F234A/L235A mutations to abrogate Fc effector function (25, 60, 61). Notably, several studies have demonstrated that the introduction of the LALA mutation leaves minimal, but sometimes detectable, Fcγ receptor binding activity (62). Since A12 only possesses the heavy-chain variable region, it completely eliminates the effector functions of the Fc region. Additionally, recent efforts have suggested that this small-sized single-domain antibody exhibited deep tissue penetration and stability. Conjugation with an Fc region increased the molecular weight, significantly diminishing tissue penetration and rendering effective inhalation unfeasible (13). Therefore, the half-life of antibody fragments can be extended significantly by fusing with a single-domain antibody targeting human serum albumin (HSA) (63), which retains the small size and feasibility for topical administration. Moreover, it has been reported that the monomeric Fc consisting of several mutants on the IgG1 Fc dimerization interface with smaller molecular (27 kDa) and enhanced tissue penetration retained the ability to bind to FcRn in pH-dependent binding ability and extend half-life (64–66).

In summary, the findings presented herein shed light on the unique properties of the UdAb A12 that specific targets IL-33. By inhibiting IL-33-induced signaling pathway, it demonstrates superior anti-inflammatory efficacy, highlighting the versatility of A12 delivery routes through inhalation or instillation and indicating the therapeutic potential in mucosal inflammation diseases. However, there are limitations to this study. Firstly, since A12 targets human IL-33 and does not bind to mouse IL-33, we used hIL-33 transgenic mice, resulting in a relatively small number of mice per group. Secondly, we used models of DED and asthma models, and will include more mucosal inflammation-related disease models to further verify the universal anti-inflammatory activity of anti-IL33 UdAb.

Materials and Methods

Study approval

All the procedures related to animal handling, care, and the treatment were performed and approved by the Ethics Committee of the School of Basic Medical Sciences at Fudan University in accordance with the recommendations in the Guide for the Care and Use of Laboratory Animals of Fudan University.

Cell culture

Human corneal epithelial cells (hCECs, donated by Professor Weiyun Shi, Qingdao, China) and Human umbilical vein endothelial cells (HUVECs, donated by Professor Changyou Zhan, Shanghai, China) were cultured in Dulbecco's modified Eagle medium (DMEM)/HAM's F12 (ThermoFisher, Waltham, MA, USA) containing 10% fetal bovine serum (ThermoFisher, Waltham, MA, USA), 100 U/mL penicillin, 100U/mL streptomycin mixture (Gibco, ThermoFisher, Waltham, MA, USA) and incubated in a 5% CO2 incubator at 37℃.

Antibody screening of anti-IL-33 UDAbs from phage libraries

The panning antigen IL-33-Biotin (109–270) protein was purchased from Acro (ACROBiosystems, Beijing, China). The fully human single-domain antibody library was constructed essentially as described previously (12). And the panning protocols also were carried out essentially as described previously. A total of 4 rounds of antibody screening were performed on biotinylated IL-33. The enrichment for antigen-specific phages after each round of panning were assessed by polyclonal phage ELISA. Positive clones expressing antibodies were identified from the enriched rounds of panning by using soluble expression-based ELISA.

Protein expression and purification

The sequences of single-domain antibodies that were positive clones in soluble expression-based ELISA were cloned into pComb3x vector with N-terminal OmpA signal peptide (MKKTAIAIAVALAGFATVAQA) and C-terminal hexahistidine and Flag tag and were expressed in *E.coli* HB2151. The expression plasmid was transformed into bacteria and a single colony was selected into the SB medium containing 100 μg/μL ampicillin. When the SB medium was cultured to A600nm ~ 0.6, 1 mM isopropyl β-D-1-thiogalactopyranoside (IPTG, Yeasen Biotechnology, Shanghai, China) was added to induce expression. After 16 h expression at 30℃, bacteria were collected, resuspended in buffer A (PBS with 500 mM NaCl) and disrupted by high pressure homogenization, followed by centrifugation at 10,000g for 30 minutes. The supernatant of single-domain antibody was purified by Ni-NTA (Yeasen Biotechnology, Shanghai, China) following the manufacture's instruction. At first, the supernatant of single-domain antibody was incubated with Ni-NTA. After incubation, the resin was washed in buffer C (buffer A with 25 mM imidazole) and antibody was eluted by buffer B (buffer A with 250 mM imidazole). Finally, the antibody was changed into PBS buffer by Millipore protein ultrafiltration tube (Millipore, Bedford, MA, USA).

The DNA sequence of IL-33 (112–270) with an N-terminal 6-His tag was cloned into pET28a vector and was expressed in *E.coli* Rosetta. SB medium containing 100 μg/μL kanamycin was cultured to A600nm ~ 0.6 and 1 mM IPTG was added to induce expression. After 16 hours expression at 16 ℃, the cells were collected, resuspended in PBS buffer and disrupted by high pressure homogenization. The purification steps were the same as mentioned above.

Recombinant ST2-Fc amino acids that used for testing the binding to IL-33 was expressed in Human Embryonic Kidney (HEK) 293 Freestyle cells (ThermoFisher, Waltham, MA, USA). Amino acids of ST2 fused with the Fc fragment of human IgG1 were cloned into mammal expression vector pcDNA3.4. The plasmid was transfected into HEK293 cells and incubated at 37℃ for 4 days. The supernatant with secreted protein was collected and purified by Protein G Resin (GenScript Biotech, Nanjing, Jiangsu, China) according to the manufacture's protocol.

The sequences of heavy chain and light chain of Itepekimab were cloned into mammal expression vector PTT. And the plasmids of heavy chain and light chain at ratio 1:1 were transfected into HEK293 cells and incubated at 37℃ for 4 days. The supernatant with secreted protein was collected and purified by Protein G Resin (GenScript Biotech, Nanjing, Jiangsu, China) according to the manufacture's protocol.

Enzyme-linked immunosorbent assay (ELISA)

Costar half-area high binding assay plates (Corning Incorporated, Corning, NY, USA) were coated with purified antigen protein at 100 ng/well in PBS overnight at 4℃, and blocked with PBS buffer containing 3% milk (w/v) at 37℃. For polyclonal phage ELISA, phages from each round of panning were incubated with immobilized antigen and bound phages were detected with anti-M13-horseradish peroxidase (HRP) polyclonal antibody (Pharmacia, New York, NY, USA, Cat# 27-9421). For the purified single-domain antibody binding assay, serially diluted antibody solutions were added and incubated for 1.5 h at 37℃, and bound antibodies were detected with monoclonal anti-Flag-HRP antibody (Sigma-Aldrich, Louis, MO, USA, clone number M2). The enzyme activity was measured with the subsequent addition of substrate ABTS (ThermoFisher, Waltham, MA, USA) and signal reading was carried out at 405 nm using a Microplate Spectrophotometer (Biotek, Winooski, VT, USA).

Biolayer Interferometry (BLI) Binding Assays

BLI was carried out on an OctetRED96 device (ForteBio, Dallas, TX, USA) and assays were carried out in 96-well black plates. For the binding kinetics of single-domain antibodies with IL-33, the recombinant UdAb-Fc protein at 15 μg/mL buffered in 0.02% PBST was immobilized onto AHC biosensors (ForteBio, Dallas, TX, USA) and incubated with threefold serial dilutions of IL-33 in kinetics buffer (PBS buffer supplemented with 0.02% Tween 20). The experiments included the following steps at 37℃: (1) baseline in water (60 s); (2) immobilization of UdAb-Fc protein onto sensors (300 s); (3) baseline in kinetics buffer (60 s); (4) association of IL-33 for measurement of k_{on} (300 s); and (5) dissociation of IL-33 for measurement of k_{off} (300 s).

All the curves were fitted by a 1:1 binding model using the Data Analysis software (ForteBio, Dallas, TX, USA). Mean k_{on}, k_{off}, and K_D values were determined by averaging binding curves within a dilution series having R^2 values of greater than 95% confidence level.

Dynamic light scattering (DLS)

For analysis of aggregation tendency of UdAbs, the UdAbs protein samples were centrifuged at 12 000 × g for 20 minutes to remove precipitates. The supernatants were filtered through a 0.45 µm filter and diluted to 1 mg/mL. Measurements were performed on a Zetasizer Nano ZS ZEN3600 (Malvern Instruments Limited, Westborough, MA, USA) according to the manufacturer's instructions. Each sample was measured three times.

Size-exclusion-high-performance liquid chromatography (SEC-HPLC)

Fifty µg of A12 were applied to a TSK-Gel Super G3000SW (Tosoh Bioscience, Griesheim, Hesse, Germany) using Waters AQUITY UPLC H-class system. The mobile phase was PBS buffer (pH 7.4) run at a flow rate of 0.4 mL/min. Absorbance was monitored at 280 nm. The UV trace was analyzed and integrated by area under the curve to determine percent aggregation, monomer and degradants.

Hydrophobicity determination of UdAbs by HIC-HPLC

Hydrophobicity of UdAbs were analyzed by HIC-HPLC. HIC-HPLC was carried out using a butylnonporous resin (NPR) column (4.6 mm inner diameter [I.D.] × 10 cm, Tosoh Corporation) with running buffer 20 mM phosphate buffer, 1.5 M $(NH4)_2SO_4$, pH 7.0 (mobile phase A), and 20 mM phosphate buffer, 25% isopropanol, pH 7.0 (mobile phase B). A total of 50 µg UdAbs or IgG (Itepekimab and Trastuzumab) was loaded and eluted at a flow rate of 10 mL/min with a gradient of 100% A to 100% B over 2 min. The detection mode used was absorbance at 280 nm.

Determination of Melting (T_m), Onset (T_{onset}) and Aggregation (T_{agg}) Temperatures

Thermal stability of UdAbs was assessed by using an Uncle/UNit system (Unchained Labs, Pleasanton, CA). Briefly, the static light scattering (SLS) at 473 nm was used as an indicator for colloidal stability, reporting the onset of aggregation temperature (Tagg), which can be defined as the temperature at which the measured scatter reaches a threshold that is approximately 10% of its maximum value. The changes in the SLS signal represented changes in the average molecular mass observed due to protein aggregation. Thermal stability was evaluated at an intrinsic fluorescence intensity ratio (350/330 nm) by measuring the temperature of the on-set of melting. The UdAbs at a concentration of 5 mg/mL were heated from 20℃ to 95℃ using 1℃ increments, with an equilibration time of 60 s before each measurement. Measurements were made in duplicates.

Binding Competition Assays

The epitopes of antibodies to IL-33 were analyzed by BLI. Sensor tips loaded with IL-33 (15 μg/mL), were immersed into wells containing the first competing antibody or ST2 at a concentration (200 nM) necessary to reach binding saturation after 300 s. Next, biosensors were dipped into wells containing the same concentration antibody or ST2 with antibody (500 nM for A12, 200 nM for Itepekimab), or only ST2 (200 nM), and binding was measured after 300 s of association. The signal obtained for binding of the second antibody in the presence of the first antibody was expressed as a percentage of the uncompeted binding of the second antibody that was derived independently. Based on the previous experimental method (12), we categorized the antibodies into competitive, intermediate competition and non-competitive. The antibodies were defined as competing if the presence of first antibody reduced the signal of the second antibody to less than 30% of its maximal binding capacity, and non-competing when binding was greater than 70%. A level of 30–69% was considered intermediate competition.

Inhibition of IL1RAcP to IL-33-ST2 binary complex

Inhibition of IL1RAcP to IL-33-ST2 binary complex by antibodies was determined by BLI. Sensor tips loaded with IL-33 (15 μg/mL), were immersed into wells containing ST2 (200 nM), or mixture of ST2 (200 nM) with A12 (300 nM), or mixture of ST2 (200 nM) with Itepekimab (200 nM) necessary to reach binding saturation after 300 s. Next, biosensors were dipped into wells containing the same concentration IL1RAcP (200 nM).

Assays of NFκB activation

HUVECs were stimulated with a constant concentration of IL-33 with or without antibodies (A12, ST2 or Itepekimab) for 30 minutes. Then, the cells were fixed with 4% PFA and blocked, and stained with Rabbit-anti-NFkB antibody (ABclonal, Wuhan, Hubei, China, clone number ARC51086). After washed, the cells were incubated with Alexa Fluor 488 conjugated goat anti-Rabbit IgG (ThermoFisher, Waltham, MA, USA). After washed, nuclei were stained with DAPI. Finally, the confocal images were recorded with a Leica confocal microscope and processed with LAS AF Lite software.

Administration of A12 to hyperosmotic model of HCECs

Hyperosmotic medium (HS) at 500 mOsm was applied to generate inflammatory stress in HCECs. HCECs were seed in 96-well plates at a density of $1x10^4$ per well or 6-well plates at a density of 1.5×10^5 per well. After HCECs reached 50% confluent, cells in 96-well plates were treated with HS, and HS with a high dose of A12 (2 μg/mL) or Itepekimab (2 μg/mL) and a low dose of A12 (0.2 μg/mL). After 15 minutes or 24 hours, supernatants were collected for ELISA assay and after 24 hours, cells viabilities were measured with Cell counting kit-8 (CCK-8) assay (Dojindo Laboratories, Kamimashiki-gun, Kumamoto, Japan). Cells in 6-well plates were treated with HS, HS with a high dose of A12 (2 μg/mL) or a low dose of A12 (0.2 μg/mL), and harvested at 0 (before stimulation), 15 minutes and 24 hours for real-time PCR and in each point supernatants of hCECs for detection of IL-33 protein by ELISA.

Determination of IL-33 levels in supernatants by ELISA kit

The supernatants of HCECs were analyzed with commercially available ELISA kits (Multi Science, Hangzhou, Zhejiang, China) in accordance with the manufacturer's instructions to determine the concentration of IL-33. In brief, each 100 μL sample was mixed with 50 μL of antibody in the wells of a precoated microplate, and then incubated for 2 h at room temperature on a plate shaker set to 100 rpm. The plates were washed 6 times with wash buffer. Then, adding 100 μL of streptavidin-HRP solution to each well and incubated the samples for 45 minutes on a plate shaker set to 100 rpm and washed 6 times with wash buffer. Subsequently, 100 μL of TMB solution was added into each well and incubated for 10 minutes in the dark before adding 100 μL of stop solution. The microplate was read with a microplate reader, and absorbance measured was 450 nm, reference at 570 nm.

Penetration experiments of single-domain antibody

Penetration experiments were carried out as described previously with minor modifications (34). 120 μL of fully human single-domain antibody A12 or Itepekimab labeled by DyLight 650 antibody Labeling Kit (ThermoFisher, Waltham, MA, USA) at 2 mg/mL in the presence of 0.1% benzalkonium chloride was added into a well of ninety-six well plate. After anesthesia, the eye of wild type C57BL/6 mice (SiPeiFu, Beijing, China) were enucleated and rinsed in PBS twice before incubation in well. After 12 hours, eyeballs were carefully taken out from the well and rinsed in PBS twice for fluorescence imaging. Eyeballs were fixed in 4% PFA for 24hours and embedded in optimum cutting temperature (OCT) (SAKURA, Torrance, CA, USA). The 10 μm frozen slices were freshly sectioned and then observed under a confocal fluorescence microscope at 650 nm.

Bio-distribution of single-domain antibody by topical instillation

Fully human single-domain antibody A12 or Itepekimab labeled by DyLight 650 antibody Labeling Kit (ThermoFisher, Waltham, MA, USA) at 3 mg/mL was administrated by instillation of 5 μL on the eye of wild type C57BL/6 mice (SiPeiFu, Beijing, China). Mice were executed at distinct time points (0, 5, 10, 15, 30, 60 minutes) precisely after administration, soon after which their eyeballs were carefully taken out from orbits and rinsed in PBS twice for fluorescence imaging. Eyeballs were fixed in 4% PFA for 24hours and embedded in optimum cutting temperature (OCT) (SAKURA, Torrance, CA, USA). The 10 μm frozen slices were freshly sectioned and then observed under a confocal fluorescence microscope at 650 nm.

The pharmacokinetic of antibody in mice by topical instillation

The single-domain antibody A12 and IgG Itepekimab were administrated by topical instillation at 15 mg/mL. after antibody administration, two mice were sacrificed to collect eye at indicated time-points. The eye was weighed, homogenized and then centrifuged at 12,000 rpm. The supernatant was harvested and stored at -80℃ for further quantified.

Antibody concentration in eye was determined by ELISA. In brief, IL-33 or anti-hFc antibody at 100 ng per well was coated in 96 well half-area microplate (Corning Incorporated, Corning, NY, USA) over night at 4℃. The antigen coated plate was blocked with PBS containing 5% BSA for 1 h at 37℃ and washed by three times of PBST (PBS with 0.05% Tween 20). 50 µL of eye homogenate in PBS at a dilution of 1:2 was added for binding at 37℃ for 1.5 h. The plate was washed with PBST for three times and incubated with anti-Flag-HRP (Sigma-Aldrich, Louis, MO, USA, clone number M2) or anti-Fab-HRP (ThermoFisher, Waltham, MA, USA) for 45 minutes at 37℃. The plate was washed with PBST for five times and the enzyme activity was measured by recording the absorbance at 405 nm after incubation with ABTS substrate (ThermoFisher, Waltham, MA, USA) for 10 minutes. Gradient serially diluted purified antibodies were used to generate quantitative standard curve and fitted by a four-parameter logistic model. The antibody concentration in eye was calculated from the standard curve.

Dry eye model mice

As human and mouse IL-33 exhibit a 55% identity at the amino acid level (16) and considering the specificity of A12 binding to human IL-33, the human IL-33 transgenic mice were opted according to previous study (25). Ten hIL-33 transgenic mice (C57BL/6-IL-33$^{tm1(hIL-33)}$, female, 8 weeks, 20 ± 2 g) were purchased from BIOCYTOGEN (BIOCYTOGEN, Beijing, China). Two mice (4 eyes) housed in a standard environment (temperature: 25°C; relative humidity: 60%) and did not treat set as blank control (n = 2, 4 eyes). Controlled environment chamber (CEC) was used to induce experimental DED in mice as described previously(67). Briefly, the CEC allows a continuous regulation and maintenance of the temperature (21℃–23℃), relative humidity (< 20%), and airflow (15 L/min). Mice were exposed to the CEC for 2 weeks. Then, eight mice were randomly divided into dry eye group and A12 treatment group (n = 4, 8 eyes) and received topical instillation of 5 µL of PBS or A12 (60 mg/mL) three times a day respectively continuously for 7 days and observed for another 7 days. At day 28, the eyeball and cervical draining lymph nodes (DLNs) were collected.

Detection of Basal Tear Secretion (Schirmer I Test)

Schirmer I was measured using phenol red-impregnated cotton threads (Jing Ming Tech Co., Ltd, Tianjing, China) at 5 p.m. to keep same time on days 0, 3, 5, 7 and 14 (one week after treatment, 2 weeks after modeling). After general anesthesia, the cotton thread was put onto lower eyelid conjunctiva near the canthus for 20 s. The length of the reddened part of the cotton thread was measured.

Corneal Fluorescein Sodium Staining Score

A total of 5 µL of 1% sodium fluorescein (w/v) was instilled into the lateral conjunctival sac to evaluate the degree of corneal epithelium defects in the mice. The corneal epithelial was visualized by a cobalt blue filter under a slit lamp microscope. Each cornea was divided into 4 quadrants and were scored separately by a masked observer using the four-point scale (0–4): 0 points, no staining; 1 point, < 30% stained dots; 2 points, > 30% non-diffuse stained dots; 3 points, severe diffuse staining but without plaque staining; 4 points, positive fluorescein plaque. The final score was obtained by adding scores from each quadrant (0–16).

Safety Evaluation

Cadaveric human corneoscleral rim were obtained from fresh cadavers and were supplied by the Eye Bank of the Eye, Ear, Nose and Throat Hospital, Fudan University, under the approval of the hospital ethics committee. Tissues used for experiments did not meet the criteria for clinical use. The corneoscleral rim was cut into small 2 mm × 1 mm pieces and randomly divided into five groups, placed in Optisol, 10% DMSO, or A12 (10 mg/mL, 60 mg/mL and 100 mg/mL respectively) at 4°C. 10% DMSO group was set as positive control. After 24 hours, the tissues were harvested for further TUNEL assay.

Immunofluorescence and TUNEL Assay

After anesthesia, the eyeballs or lung tissues collected from the mice or human corneoscleral pieces were placed in 4% paraformaldehyde (PFA) for overnight fixation and then made into 10 μm paraffin sections. For paraffin sections processed for immunofluorescence and TUNEL assay. Sections were deparaffinized, rehydrated and underwent antigen retrieval. Then, slides were dried at room temperature for 20 minutes and washed with PBS solution for 3 times. Then, the slides were incubated in 0.1% Triton X-100 (prepared in PBS) for 15 minutes periods. As slides for TUNEL assay, a commercial kit (In Situ Cell Death Detection Kit, Roche Diagnostics, Indianapolis, IN, USA) was used following instructions.

For Immunofluorescence staining, slides were blocked in blocking buffer with 3% BSA in a humidified box at room temperature for 30 minutes. Slides were incubated with primary antibody against human IL-33 (1:100, R&D systems, Minneapolis, MN, USA) or ST2 antibody (1:200, Proteintech, Rosemont, IL, USA, clone number 7A2A7) at 4°C overnight. The slides were then incubated with an anti-goat secondary antibody (1:500, ThermoFisher, Waltham, MA, USA, clone number AB_2925786) or an anti-mouse secondary antibody (1:500, ThermoFisher, Waltham, MA, USA, clone number AB_2536180) for 1 hour. The specific antibody for macrophages were F4/80 (1:100, Biolegend, San Diego, CA, USA, clone number BM8) and slides were incubated with it for 1 hour. Finally, the nuclei were stained with DAPI. TUNEL images were taken at 10x and immunofluorescence images were taken at 40× with an oil-immersion microscope (Leica, Witzler, Hesse, Germany).

Aerodynamic particle size measured by Next Generation Impactor

To determine the size distribution of the aerosol antibodies, we used the NGI (Beijing Huironghe Technology, Beijing, China) to analyze the aerodynamic parameters of antibodies according the USP monograph. There are seven-stage droplets collectors representing different cutoff diameters of collected particles in the NGI located in its bottom frame. 4 mg/mL A12 and IgG Itepekimab were aerosolized and deposited on different collection cups at ambient room conditions within 180 s. Specifically, after the assembly was set up and airtight checked followed by vacuum pump running at the constant flow rates of 15 L/min, the antibody solution was added and fired into the cascade impactor immediately. Droplets of each collection plate was washed and collected by 0.02% PBST, and then the

components were dried up before next experiment. The concentration of antibodies in collected solution was quantified by ELISA as mentioned above.

The pharmacokinetic of antibody in mice by inhalation

The UdAb A12 and IgG Itepekimab were administrated through intratracheal route using microsprayer aerosolizer (YUYANBIO, Shanghai, China) at 10 mg/kg. After antibody administration, two mice were sacrificed to collect lung, trachea and blood at indicated time-points (0.5 h, 2 h, 4 h, 8 h and 12 h). The lung and trachea were weighed, homogenized and then centrifuged at 12,000 rpm to collect supernatant. Then the antibody concentration in supernatant was determined by ELISA as mentioned above.

Asthma Model Mice

Ten hIL-33 transgenic mice (C57BL/6-IL-33$^{tm1(hIL-33)}$, female, 8 weeks, 20 ± 2 g) were purchased from BIOCYTOGEN (BIOCYTOGEN, Beijing, China). The mice were housed in a standard environment with constant temperature (22 ± 1°C) and a regular light/dark (12 h/12 h) cycle with ad libitum access to food and water. The animal model of asthma and administration regimen were designed based on previously reported (68). Two mice did not be treated set as blank control (n = 2). Eight mice were sensitized intraperitoneally with 50 μg of OVA (Sigma-Aldrich, Louis, MO, USA) and 50 μL Imject Alum (ThermoFisher, Waltham, MA, USA) at day 0 and day 7. Seven days later, they were randomly divided into either OVA group or A12 group (n = 4) administrated with PBS or A12 respectively for consecutively three days. Fifteen minutes before intranasal challenge of 20 μL of 2% OVA (w/v), 50 μL A12 (10 mg/mL, 25 mg/kg) or PBS was administrated through intratracheal route using microsprayer aerosolizer (YUYANBIO, Shanghai, China)(13). Briefly, a laryngoscope was put in mice mouth to visualize the porch of the trachea, after which the tip syringe of high-pressure microsprayer was gently fed into the main trachea and infused quickly to deliver the aerosols. Mice were executed 24 hours after the last challenge. Right lung was isolated for flowcytometry, the superior lobe of left lung was cut for RT-qPCR analysis, and the inferior lobe of left lung were harvested for histology analysis. Before flow cytometric analysis, the right lung from each mouse was digested into a single-cell suspension using RPMI 1640 (Gibco, ThermoFisher, Waltham, MA, USA) solution containing 1 mg/mL collagenase IV (Yeasen Biotechnology, Shanghai, China), 20 μg/mL DNase I (Yeasen Biotechnology, Shanghai, China) and 1 mg/mL hyaluronidaseon (Yeasen Biotechnology, Shanghai, China) shake set to 100 rpm for 1 hour. Lung-draining mediastinal lymph nodes (MLNs) were also isolated for flow cytometry. Plasma was collected for detection of IgE levels.

Flow cytometric analysis

The single-cell suspension was stained with Fixable Viability Stain 780 (BD Biosciences, Allschwil, Basel, Switzerland) to allow exclusion of dead cells and anti-mouse CD16/32 to block non-specific binding of immunoglobulin to the Fc receptors (Biolegend, San Diego, CA, USA).

For dry eye experiments, to quantify mature APCs in draining lymph nodes, cells were stained with a Percp-Cy5.5 rat anti-mouse CD45 (Biolegend, San Diego, CA, USA, clone number S18009F), FITC armenian hamster anti-mouse CD11c (Biolegend, San Diego, CA, USA, clone number N418), PE-Cy7 rat anti-mouse F4/80 (Biolegend, San Diego, CA, USA, clone number BM8), PE rat anti-mouse CD86 (Biolegend, San Diego, CA, USA, clone number GL-1), Pacific blue rat anti-mouse MHC Class II (Biolegend, San Diego, CA, USA, clone number M5/114.15.2). To assess Th1 cells in DLNs, cells were stained with the following antibodies: FITC rat anti-mouse CD3 (Biolegend, San Diego, CA, USA, clone number SK7), Percp rat anti-mouse CD4 (Biolegend, San Diego, CA, USA, clone number RM4-5), PE rat anti-mouse CD8a (Biolegend, San Diego, CA, USA, clone number 53 – 6.7), Percp-Cy5.5 rat anti-mouse CD45 (Biolegend, San Diego, CA, USA, clone number S18009F) and Brilliant Violet 605™ rat anti-mouse ST2 (Biolegend, San Diego, CA, USA, clone number DIH9). After fixation and permeabilization (eBioscience, San Diego, CA, USA), cells were stained with an APC rat anti-mouse IFNγ antibody (Biolegend, San Diego, CA, USA, clone number XMG1.2).

In terms of asthma experiments, to assess eosinophil frequencies, cells were stained with the following antibodies: PE rat anti-mouse CD11b (Biolegend, San Diego, CA, USA, clone number M1/70), FITC armenian hamster anti-mouse CD11c (Biolegend, San Diego, CA, USA, clone number N418), APC rat anti-mouse Siglec-F (Biolegend, Biolegend, San Diego, CA, USA, clone number S17007L), Percp-Cy5.5 rat anti-mouse CD45 (Biolegend, San Diego, CA, USA, clone number S18009F). To quantify T cells, cells were stained with BV510 rat anti-mouse CD3 (Biolegend, San Diego, CA, USA, clone number 17A2), FITC rat anti-mouse CD4 (Biolegend, San Diego, CA, USA, clone number GK1.5), PE rat anti-mouse CD8a (Biolegend, San Diego, CA, USA, clone number 53 – 6.7), Percp-Cy5.5 rat anti-mouse CD45 (Biolegend, San Diego, CA, USA, clone number S18009F).

Appropriate isotype-matched control antibodies were used in all experiments. Stained cells were analyzed on a BD Caliber. Data analysis was performed using Flowjo 7.6.1.

IgE concentration in plasma

The IgE concentration in mice plasma was determined by ELISA (BD Biosciences, Allschwil, Basel, Switzerland). In brief, capture antibody purified anti-Mouse IgE diluted with PBS was coated in 96 well half-area microplate (Corning Incorporated, Corning, NY, USA) over night at 4℃. The antigen coated plate was blocked with PBS containing 5% BSA for 1 h at 37℃ and washed by three times of PBST (PBS with 0.05% Tween 20). 50 µL plasma at a dilution of 1:3 was added for binding at 37℃ for 1.5 hours. The plate was washed with PBST for three times and incubated with anti-Mouse-IgE-HRP (ThermoFisher, Waltham, MA, USA) for 45 minutes at 37℃. The plate was washed with PBST for five times and the enzyme activity was measured by recording the absorbance at 405 nm after incubation with ABTS substrate (Invitrogen, ThermoFisher, Waltham, MA, USA) for 10 minutes. Gradient serially diluted purified mouse IgE was used to generate quantitative standard curve and fitted by a four-parameter logistic model. The IgE concentration in plasma was calculated from the standard curve.

Quantitative real-time PCR (RT-qPCR)

Total RNA extraction, reverse transcription and quantitative real-time PCR were performed as previously described. Total RNA was extracted from hCEC cells, corneal tissue, lung or lymphoid tissues by using the TRIzol reagent (ThermoFisher, Waltham, MA, USA). After synthesized with the PrimeScript RT Master Mix (TianGen, Beijing, China), each sample of cDNA was quantitated with three replicates by RT-qPCR kit (TianGen, Beijing, China). The β-actin gene served as an internal control, and the relative mRNA level in the untreated group was regarded as the calibrator. The primers used in this study were as follows:

hActin-F: TGGCTGGGGTGTTGAAGGTCT;

hActin-R: AGCACGGCATCGTCACCAACT;

hIl-1β-F: TGGAGCAACAAGTGGTGTTC;

hIl-1β-R: GCTGTAGAGTGGGCTTATCATC;

hIl-6-F: ACTCACCTCTTCAGAACGAATTG;

hIl-6-R: CCATCTTTGGAAGGTTCAGGTTG;

hTnf-α-F: AGCCCATGTTGTAGCAAACC;

hTnf-α-R: TGAGGTACAGGCCCTCTGAT;

hIl-33-F: GTGACGGTGTTGATGGTAAGAT;

hIl-33-R: AGCTCCACAGAGTGTTCCTTG;

mActin-F: GGCTGTATTCCCCTCCATCG;

mActin-R: CCAGTTGGTAACAATGCCATGT;

mIl-6-F: CTGCAAGAGACTTCCATCCAG;

mIl-6-R: AGTGGTATAGACAGGTCTGTTGG;

mIl-1β-F: AGCTTCAGGCAGGCAGTATC;

mIl-1β-R: AAGGTCCACGGGAAAGACAC;

mTnf-α-F: CTGAACTTCGGGGTGATCGG;

mTnf-α-R: GGCTTGTCACTCGAATTTTGAGA;

mSt2-F: TGACACCTTACAAAACCCGGA;

mSt2-R: AGGTCTCTCCCATAAATGCACA;

mMuc5ac-F: GTGGTTTGACACTGACTTCCC;

mMuc5ac-R: CTCCTCTCGGTGACAGAGTCT;

mll-4-F: GGTCTCAACCCCCAGCTAGT;

mll-4-R: GCCGATGATCTCTCTCAAGTGAT;

mll-5-F: TCAGGGGCTAGACATACTGAAG;

mll-5-R: CCAAGGAACTCTTGCAGGTAAT;

mll-13-F: CAGCCTCCCCGATACCAAAAT;

mll-13-R: GCGAAACAGTTGCTTTGTGTAG.

Statistics

Statistical analysis was performed using GraphPad Prism 8.3 software. For all experiments, data are expressed as means ± SD. The statistical significance of experiments with two groups, unpaired two-tailed Student's t tests were used. One-way ANOVA followed by Tukey's post hoc test was employed to assess for multiple comparisons among the different experimental conditions to adjust the calculation power. Statistical significance levels are represented as *P < .05, **P < .01, ***P < .001, ****P < .0001 and ns, no significances.

Declarations

Data availability

All data needed to evaluate the conclusions in the paper are present in the paper and/or the Supplementary Materials.

Acknowledgements

T.Y. and YL.W. are supported by grants from the National Key R&D Program of China (2019YFA0904400), National Natural Science Foundation of China (32270984), Science and Technology Commission of Shanghai Municipality (23XD1400800), and Shanghai Municipal Health Commission (GWVI-11.2-YQ46). J.H. is supported by the National Natural Science Foundation of China (82171102, 81970766, 82271044), the National Key Research and Development Program of China (2023YFA0915000), the Shanghai Medical Innovation Research Program (22Y21900900), the Shanghai Key Clinical Research Program (SHDC2020CR3052B).

Author contributions

J.H., YL.W. and T.Y. initiated, planned and supervised the project. K.H. and YQ.W. performed most of the experiments and analyzed the data with assistance from Y.K., Q.X., Y.Z., Q.L., C.L., W.S. and X.Z. The manuscript was reviewed, commented and approved by all the authors.

Conflict of Interest

The authors declare that they have no competing interests.

References

1. de Paiva CS, St Leger AJ, Caspi RR. Mucosal immunology of the ocular surface. Mucosal Immunol. 2022;15(6):1143-57.
2. Jones RG, Martino A. Targeted localized use of therapeutic antibodies: a review of non-systemic, topical and oral applications. Crit Rev Biotechnol. 2016;36(3):506-20.
3. Brusselle GG, Koppelman GH. Biologic Therapies for Severe Asthma. N Engl J Med. 2022;386(2):157-71.
4. Weng Y, Liu J, Jin S, Guo W, Liang X, Hu Z. Nanotechnology-based strategies for treatment of ocular disease. Acta Pharm Sin B. 2017;7(3):281-91.
5. Hart TK, Cook RM, Zia-Amirhosseini P, Minthorn E, Sellers TS, Maleeff BE, et al. Preclinical efficacy and safety of mepolizumab (SB-240563), a humanized monoclonal antibody to IL-5, in cynomolgus monkeys. J Allergy Clin Immunol. 2001;108(2):250-7.
6. Parray HA, Shukla S, Perween R, Khatri R, Shrivastava T, Singh V, et al. Inhalation monoclonal antibody therapy: a new way to treat and manage respiratory infections. Appl Microbiol Biotechnol. 2021;105(16-17):6315-32.
7. Martin DF, Maguire MG, Ying GS, Grunwald JE, Fine SL, Jaffe GJ. Ranibizumab and bevacizumab for neovascular age-related macular degeneration. N Engl J Med. 2011;364(20):1897-908.
8. de Cogan F, Hill LJ, Lynch A, Morgan-Warren PJ, Lechner J, Berwick MR, et al. Topical Delivery of Anti-VEGF Drugs to the Ocular Posterior Segment Using Cell-Penetrating Peptides. Invest Ophthalmol Vis Sci. 2017;58(5):2578-90.
9. Shettle L, McLaurin E, Martel J, Seaman JW, 3rd, Weissgerber G. Topical Anti-TNFα Agent Licaminlimab (OCS-02) Relieves Persistent Ocular Discomfort in Severe Dry Eye Disease: A Randomized Phase II Study. Clin Ophthalmol. 2022;16:2167-77.
10. Morrison C. Nanobody approval gives domain antibodies a boost. Nat Rev Drug Discov. 2019;18(7):485-7.
11. Muyldermans S. Nanobodies: natural single-domain antibodies. Annu Rev Biochem. 2013;82:775-97.
12. Wu Y, Li C, Xia S, Tian X, Kong Y, Wang Z, et al. Identification of Human Single-Domain Antibodies against SARS-CoV-2. Cell Host Microbe. 2020;27(6):891-8.e5.
13. Li C, Zhan W, Yang Z, Tu C, Hu G, Zhang X, et al. Broad neutralization of SARS-CoV-2 variants by an inhalable bispecific single-domain antibody. Cell. 2022;185(8):1389-401.e18.

14. Wu Y, Li Q, Kong Y, Wang Z, Lei C, Li J, et al. A highly stable human single-domain antibody-drug conjugate exhibits superior penetration and treatment of solid tumors. Mol Ther. 2022;30(8):2785-99.
15. Kolkhir P, Akdis CA, Akdis M, Bachert C, Bieber T, Canonica GW, et al. Type 2 chronic inflammatory diseases: targets, therapies and unmet needs. Nat Rev Drug Discov. 2023;22(9):743-67.
16. Schmitz J, Owyang A, Oldham E, Song Y, Murphy E, McClanahan TK, et al. IL-33, an interleukin-1-like cytokine that signals via the IL-1 receptor-related protein ST2 and induces T helper type 2-associated cytokines. Immunity. 2005;23(5):479-90.
17. Qian Y, Zhang M. The Functional Roles of IL-33/ST2 Axis in Ocular Diseases. Mediators Inflamm. 2020;2020:5230716.
18. Moussion C, Ortega N, Girard JP. The IL-1-like cytokine IL-33 is constitutively expressed in the nucleus of endothelial cells and epithelial cells in vivo: a novel 'alarmin'? PLoS One. 2008;3(10):e3331.
19. Yi XM, Li M, Chen YD, Shu HB, Li S. Reciprocal regulation of IL-33 receptor-mediated inflammatory response and pulmonary fibrosis by TRAF6 and USP38. Proc Natl Acad Sci U S A. 2022;119(10):e2116279119.
20. Préfontaine D, Lajoie-Kadoch S, Foley S, Audusseau S, Olivenstein R, Halayko AJ, et al. Increased expression of IL-33 in severe asthma: evidence of expression by airway smooth muscle cells. J Immunol. 2009;183(8):5094-103.
21. Saikumar Jayalatha AK, Hesse L, Ketelaar ME, Koppelman GH, Nawijn MC. The central role of IL-33/IL-1RL1 pathway in asthma: From pathogenesis to intervention. Pharmacol Ther. 2021;225:107847.
22. Tang S, Huang H, Hu F, Zhou W, Guo J, Jiang H, et al. Increased IL-33 in synovial fluid and paired serum is associated with disease activity and autoantibodies in rheumatoid arthritis. Clin Dev Immunol. 2013;2013:985301.
23. Byers DE, Alexander-Brett J, Patel AC, Agapov E, Dang-Vu G, Jin X, et al. Long-term IL-33-producing epithelial progenitor cells in chronic obstructive lung disease. J Clin Invest. 2013;123(9):3967-82.
24. Wang S, Zhang H. Upregulation of the IL-33/ST2 pathway in dry eye. Mol Vis. 2019;25:583-92.
25. Allinne J, Scott G, Lim WK, Birchard D, Erjefält JS, Sandén C, et al. IL-33 blockade affects mediators of persistence and exacerbation in a model of chronic airway inflammation. J Allergy Clin Immunol. 2019;144(6):1624-37.e10.
26. England E, Rees DG, Scott IC, Carmen S, Chan DTY, Chaillan Huntington CE, et al. Tozorakimab (MEDI3506): an anti-IL-33 antibody that inhibits IL-33 signalling via ST2 and RAGE/EGFR to reduce inflammation and epithelial dysfunction. Sci Rep. 2023;13(1):9825.
27. Wechsler ME, Ruddy MK, Pavord ID, Israel E, Rabe KF, Ford LB, et al. Efficacy and Safety of Itepekimab in Patients with Moderate-to-Severe Asthma. N Engl J Med. 2021;385(18):1656-68.
28. Carriere V, Roussel L, Ortega N, Lacorre DA, Americh L, Aguilar L, et al. IL-33, the IL-1-like cytokine ligand for ST2 receptor, is a chromatin-associated nuclear factor in vivo. Proc Natl Acad Sci U S A.

2007;104(1):282-7.
29. Dwyer GK, D'Cruz LM, Turnquist HR. Emerging Functions of IL-33 in Homeostasis and Immunity. Annu Rev Immunol. 2022;40:15-43.
30. Liew FY, Girard JP, Turnquist HR. Interleukin-33 in health and disease. Nat Rev Immunol. 2016;16(11):676-89.
31. Chen Y, Wang S, Alemi H, Dohlman T, Dana R. Immune regulation of the ocular surface. Exp Eye Res. 2022;218:109007.
32. Ma B, Zhou Y, Liu R, Zhang K, Yang T, Hu C, et al. Pigment epithelium-derived factor (PEDF) plays anti-inflammatory roles in the pathogenesis of dry eye disease. Ocul Surf. 2021;20:70-85.
33. Mandal A, Pal D, Agrahari V, Trinh HM, Joseph M, Mitra AK. Ocular delivery of proteins and peptides: Challenges and novel formulation approaches. Adv Drug Deliv Rev. 2018;126:67-95.
34. Ottiger M, Thiel MA, Feige U, Lichtlen P, Urech DM. Efficient intraocular penetration of topical anti-TNF-alpha single-chain antibody (ESBA105) to anterior and posterior segment without penetration enhancer. Invest Ophthalmol Vis Sci. 2009;50(2):779-86.
35. Singh RB, Blanco T, Mittal SK, Taketani Y, Chauhan SK, Chen Y, et al. Pigment Epithelium-derived Factor secreted by corneal epithelial cells regulates dendritic cell maturation in dry eye disease. Ocul Surf. 2020;18(3):460-9.
36. Galletti JG, Guzmán M, Giordano MN. Mucosal immune tolerance at the ocular surface in health and disease. Immunology. 2017;150(4):397-407.
37. Barabino S, Chen Y, Chauhan S, Dana R. Ocular surface immunity: homeostatic mechanisms and their disruption in dry eye disease. Prog Retin Eye Res. 2012;31(3):271-85.
38. Maruoka S, Inaba M, Ogata N. Activation of Dendritic Cells in Dry Eye Mouse Model. Invest Ophthalmol Vis Sci. 2018;59(8):3269-77.
39. Tan X, Chen Y, Foulsham W, Amouzegar A, Inomata T, Liu Y, et al. The immunoregulatory role of corneal epithelium-derived thrombospondin-1 in dry eye disease. Ocul Surf. 2018;16(4):470-7.
40. Bron AJ, de Paiva CS, Chauhan SK, Bonini S, Gabison EE, Jain S, et al. TFOS DEWS II pathophysiology report. Ocul Surf. 2017;15(3):438-510.
41. Papi A, Brightling C, Pedersen SE, Reddel HK. Asthma. Lancet. 2018;391(10122):783-800.
42. Moffatt MF, Gut IG, Demenais F, Strachan DP, Bouzigon E, Heath S, et al. A large-scale, consortium-based genomewide association study of asthma. N Engl J Med. 2010;363(13):1211-21.
43. Patton JS, Byron PR. Inhaling medicines: delivering drugs to the body through the lungs. Nat Rev Drug Discov. 2007;6(1):67-74.
44. Jin G, Liu Y, Wang L, He Z, Zhao X, Ma Y, et al. A single infusion of engineered long-lived and multifunctional T cells confers durable remission of asthma in mice. Nat Immunol. 2024;25(6):1059-72.
45. Udpa N, Million RP. Monoclonal antibody biosimilars. Nat Rev Drug Discov. 2016;15(1):13-4.

46. Singh S, Kumar NK, Dwiwedi P, Charan J, Kaur R, Sidhu P, et al. Monoclonal Antibodies: A Review. Curr Clin Pharmacol. 2018;13(2):85-99.
47. Mullard A. FDA approves 100th monoclonal antibody product. Nat Rev Drug Discov. 2021;20(7):491-5.
48. Lo KM, Leger O, Hock B. Antibody Engineering. Microbiol Spectr. 2014;2(1):Aid-0007-2012.
49. Dastjerdi MH, Sadrai Z, Saban DR, Zhang Q, Dana R. Corneal penetration of topical and subconjunctival bevacizumab. Invest Ophthalmol Vis Sci. 2011;52(12):8718-23.
50. Holgado A, Braun H, Van Nuffel E, Detry S, Schuijs MJ, Deswarte K, et al. IL-33trap is a novel IL-33-neutralizing biologic that inhibits allergic airway inflammation. J Allergy Clin Immunol. 2019;144(1):204-15.
51. Galletti JG, de Paiva CS. Age-related changes in ocular mucosal tolerance: Lessons learned from gut and respiratory tract immunity. Immunology. 2021;164(1):43-56.
52. Bron AJ, de Paiva CS, Chauhan SK, Bonini S, Gabison EE, Jain S, et al. Corrigendum to "TFOS DEWS II pathophysiology report" [Ocul. Surf. 15 (3) (2017) 438-510]. Ocul Surf. 2019;17(4):842.
53. Lin J, Zhao GQ, Wang Q, Xu Q, Che CY, Hu LT, et al. Regulation of interleukin 33/ST2 signaling of human corneal epithelium in allergic diseases. Int J Ophthalmol. 2013;6(1):23-9.
54. Na KS, Mok JW, Kim JY, Rho CR, Joo CK. Correlations between tear cytokines, chemokines, and soluble receptors and clinical severity of dry eye disease. Invest Ophthalmol Vis Sci. 2012;53(9):5443-50.
55. Chen H, Gan X, Li Y, Gu J, Liu Y, Deng Y, et al. NLRP12- and NLRC4-mediated corneal epithelial pyroptosis is driven by GSDMD cleavage accompanied by IL-33 processing in dry eye. Ocul Surf. 2020;18(4):783-94.
56. Hu J, Gao N, Zhang Y, Chen X, Li J, Bian F, et al. IL-33/ST2/IL-9/IL-9R signaling disrupts ocular surface barrier in allergic inflammation. Mucosal Immunol. 2020;13(6):919-30.
57. Wang HH, Chen WY, Huang YH, Hsu SM, Tsao YP, Hsu YH, et al. Interleukin-20 is involved in dry eye disease and is a potential therapeutic target. J Biomed Sci. 2022;29(1):36.
58. Jackson DJ, Makrinioti H, Rana BM, Shamji BW, Trujillo-Torralbo MB, Footitt J, et al. IL-33-dependent type 2 inflammation during rhinovirus-induced asthma exacerbations in vivo. Am J Respir Crit Care Med. 2014;190(12):1373-82.
59. Rabe KF, Celli BR, Wechsler ME, Abdulai RM, Luo X, Boomsma MM, et al. Safety and efficacy of itepekimab in patients with moderate-to-severe COPD: a genetic association study and randomised, double-blind, phase 2a trial. Lancet Respir Med. 2021;9(11):1288-98.
60. Wang X, Mathieu M, Brezski RJ. IgG Fc engineering to modulate antibody effector functions. Protein Cell. 2018;9(1):63-73.
61. Okragly AJ, Corwin KB, Elia M, He D, Schroeder O, Zhang Q, et al. Generation and Characterization of Torudokimab (LY3375880): A Monoclonal Antibody That Neutralizes Interleukin-33. J Inflamm Res. 2021;14:3823-35.

62. Eroshenko N, Gill T, Keaveney MK, Church GM, Trevejo JM, Rajaniemi H. Implications of antibody-dependent enhancement of infection for SARS-CoV-2 countermeasures. Nat Biotechnol. 2020;38(7):789-91.
63. Meetze K, Mehta NK, Li B, Michaelson JS, Baeuerle PA. CLN-978, a novel half-life extended CD19/CD3/HSA-specific T cell-engaging antibody construct with potent activity against B-cell malignancies with low CD19 expression. J Immunother Cancer. 2023;11(8).
64. Ying T, Gong R, Ju TW, Prabakaran P, Dimitrov DS. Engineered Fc based antibody domains and fragments as novel scaffolds. Biochim Biophys Acta. 2014;1844(11):1977-82.
65. Ying T, Ju TW, Wang Y, Prabakaran P, Dimitrov DS. Interactions of IgG1 CH2 and CH3 Domains with FcRn. Front Immunol. 2014;5:146.
66. Wang C, Wu Y, Wang L, Hong B, Jin Y, Hu D, et al. Engineered Soluble Monomeric IgG1 Fc with Significantly Decreased Non-Specific Binding. Front Immunol. 2017;8:1545.
67. Barabino S, Shen L, Chen L, Rashid S, Rolando M, Dana MR. The controlled-environment chamber: a new mouse model of dry eye. Invest Ophthalmol Vis Sci. 2005;46(8):2766-71.
68. Wang J, Gao S, Zhang J, Li C, Li H, Lin J. Interleukin-22 attenuates allergic airway inflammation in ovalbumin-induced asthma mouse model. BMC Pulm Med. 2021;21(1):385.

Figures

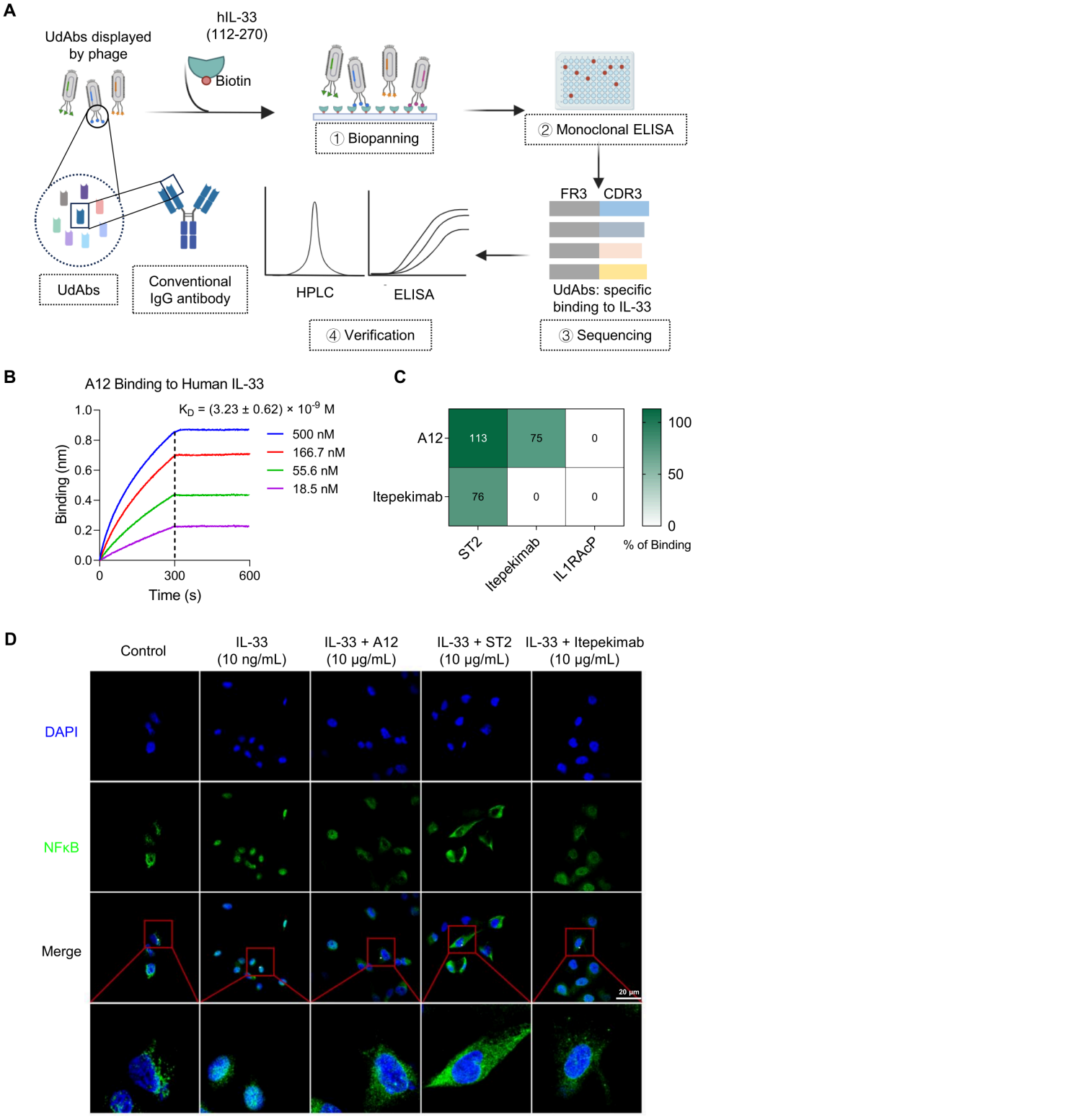

Figure 1

Identification and characterization of fully human single-domain antibodies (UdAbs) targeting IL-33.

A. Screening strategy of anti-IL-33 fully human single-domain antibodies by phage display library. In brief, four rounds of UdAb screening were performed on biotinylated IL-33. The enrichment for antigen-specific

clones were assessed by monoclonal ELISA after the fourth round. Then the positive clones were sequenced and purified for the further verification.

B. Binding affinity of A12 to IL-33 by BLI, the K_D value is shown.

C. Competition of antibodies (A12 and Itepekimab) with ST2 for IL-33 binding and with each other and inhibition of IL1RAcP to IL-33-ST2 binary complex by antibodies were determined by BLI. The values are the percentage of binding that occurred during competition in comparison with non-competed binding, which was normalized to 100%, and the range of competition is indicated by the box colors. Residual binding <30% indicates strongly competing pairs, residual binding 30%–70% indicates intermediate competition, and residual binding >70% indicates non-competing pairs.

D. The inhibition of IL-33 induced NFκB activity by antibodies determined by immunofluorescence staining, DAPI (blue), NFκB (green).

Figure 2

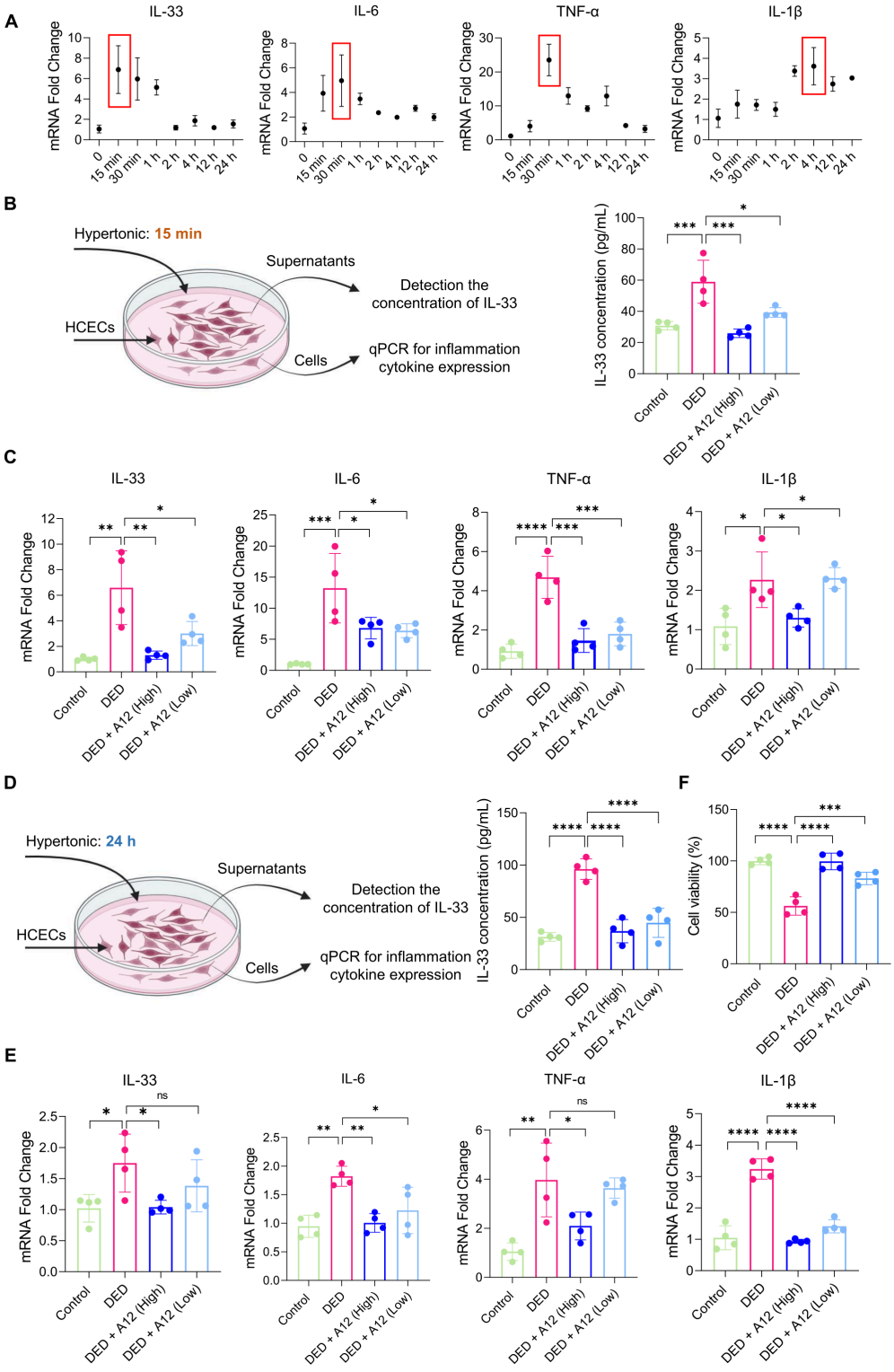

Figure 2

Anti-inflammatory effect of A12 *in vitro.*

A. HCECs were treated with 500 mOsm HS medium to induced DED. And the expression of the inflammatory cytokines in HCECs, including IL-33, IL-6, TNF-α, IL-1β at different time post hyperosmotic

stress: 0 min 15 min, 30 min, 1 h, 2 h, 4 h, 12 h and 24 h, was analyzed by RT-qPCR. Red rectangle indicated the peak expression of mRNA levels.

B. Schematic diagram of 500 mOsm hyperosmotic medium (HS) medium induced DED, where HCECs were treated with high-dose of A12 (2 μg/mL) or a low dose of A12 (0.2 μg/mL). HCECs under physiological osmotic pressure were set as control (n=4). After 15 minutes 500 mOsm HS stimulation, IL-33 concentration in supernatants of HCECs was analyzed by ELISA.

C. Expression mRNA levels of the inflammatory cytokines in HCECs 15 minutes post hyperosmotic stress.

D. Schematic diagram of 500 mOsm HS medium induced DED for 24 hours.

E. Expression of the inflammatory cytokines in HCECs, including IL-33, IL-6, TNF-α, IL-1β after hyperosmotic stress 24 h.

F. Cell viability measured by CCK-8 assay.

Results are representative of 2 independent experiments. Error bars represent means ± SD. One-way ANOVA followed by Tukey's post hoc test was employed to assess for multiple comparisons among the different experimental conditions to adjust the calculation power. Statistical significance levels are represented as *P < .05, **P < .01, ***P < .001, ****P < .0001 and ns, no significances.

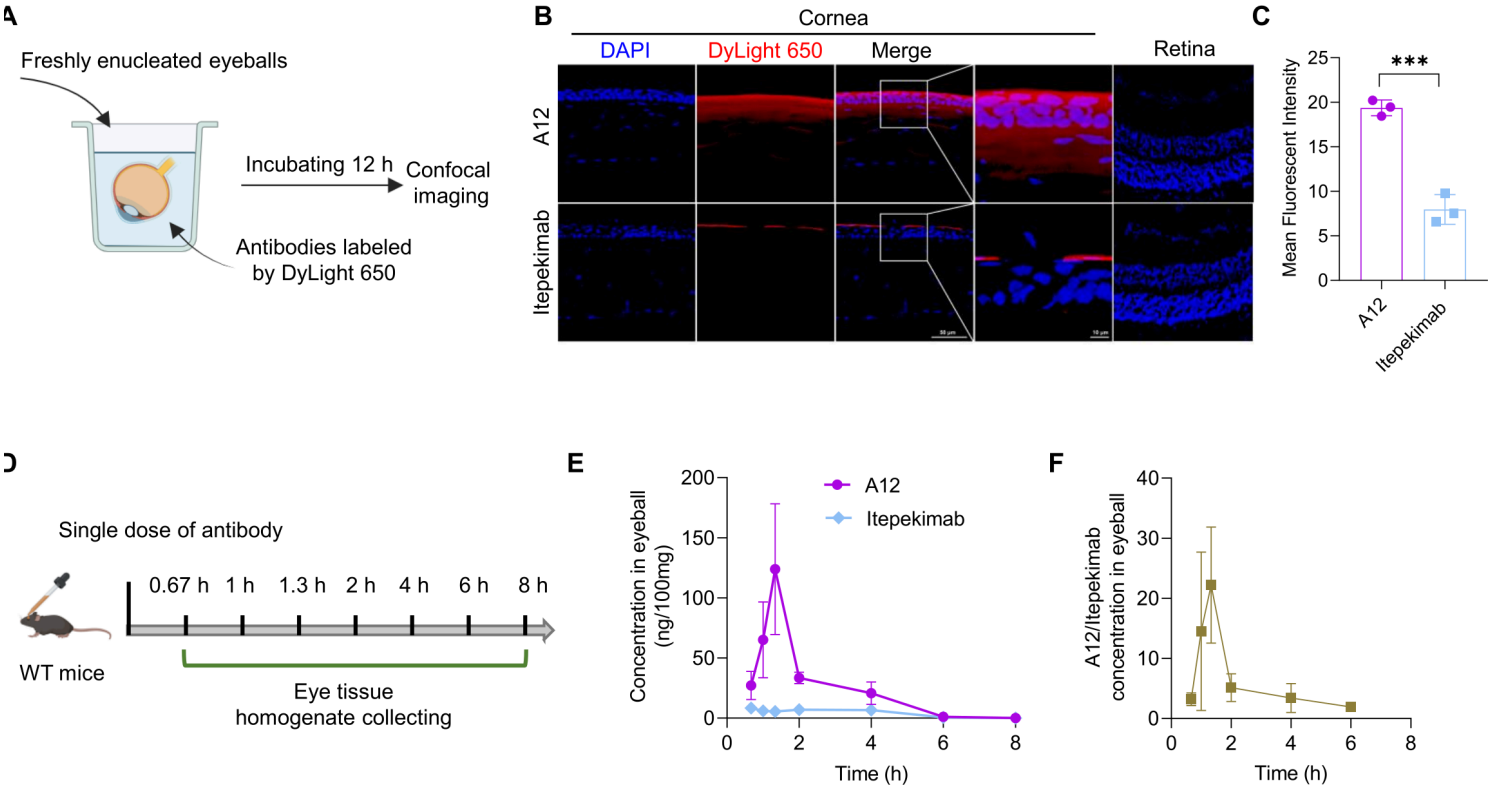

Figure 3

Bio-distribution of A12 and Itepekimab *in vivo.*

A. Schematic diagram of antibody penetration experiments.

B-C. Fluorescence signal (E) and intensity (F) in cornea and retina of mice after incubation 12 hours in 2 mg/mL A12 or Itepekimab in the presence of 0.1% benzalkonium chloride. The scale bar is 50 μm.

D. Schematic diagram of A12 biodistribution in mice by instillation.

E-F. Eyeballs treated by topical instillation of A12 or Itepekimab were harvested at different time point for homogenate, and then determined the concentration of antibodies by ELISA.

Results are representative of 2 independent experiments. Error bars represent means ± SD. Unpaired two-tailed Student's t tests were used in the statistical analysis. Statistical significance levels are represented as *P < .05, **P < .01, ***P < .001, ****P < .0001 and ns, no significances.

Figure 4

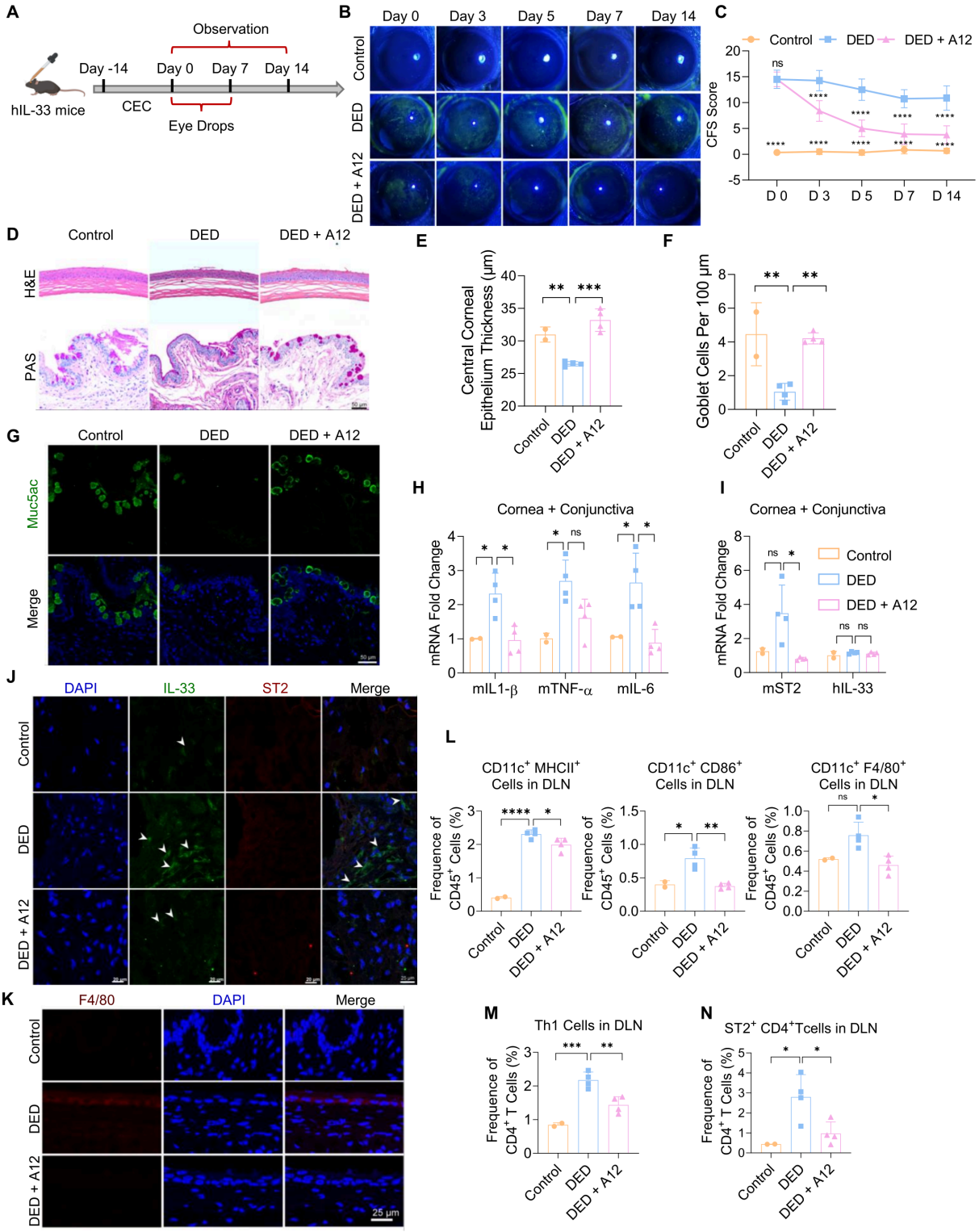

Figure 4

Instillation of A12 downregulates inflammation in CEC-induced dry eye disease.

A. Schematic diagram of therapeutic procedure of A12 on DED. Naïve C57BL/6-IL-33$^{tm1(hIL-33)}$ mice were set as control.

B-C. Representative fluorescein sodium staining images and corresponding staining scores. (For control, DED and DED + A12 mouse models, n = 4, 8 and 8, respectively, n: number of eyeballs)

D. Representative H&E staining images of the cornea and conjunctival PAS staining images. The scale bar is 50 μm. (For control, DED and DED + A12 mouse models, n = 2, 4 and 4, respectively, n: number of eyeballs)

E. Quantitative analysis of the corneal epithelial thickness.

F. Quantitative analysis of goblet cell number per 100 μm.

G. Immunofluorescence staining of Muc5AC in conjunctiva of mice in DED modeling

H. Expression of inflammatory cytokine mRNA levels, including *mIl-1β*, *mTnf-α* and *mIl-6* detected by RT-qPCR in cornea and conjunctiva. (For control, DED and DED + A12 mouse models, n = 2, 4 and 4, respectively, n: number of eyeballs)

I. Expression of *mST2* and human *IL-33* mRNA levels in cornea and conjunctiva. (For control, DED and DED + A12 mouse models, n = 2, 4 and 4, respectively, n: number of eyeballs)

J. Immunofluorescence staining of hIL-33 and mST2 in conjunctiva in DED modeling. (For control, DED and DED + A12 mouse models, n = 2, 4 and 4, respectively, n: number of eyeballs)

K. Evaluations of $F4/80^+$ cells by immunostaining on the conjunctival. The scale bars are 50 μm.

L. Representative flow cytometry plots and frequencies of $CD11c^+MHC\text{□}^+$DCs, $CD11c^+CD86^+$ DCs (k), and $CD11c^+F4/80^+$ macrophages in the DLNs. (For control, DED and DED + A12 mouse models, n = 2, 4 and 4, respectively, n: number of mice)

M-N. Frequencies of Th1 cells (m)and $ST2^+$ $CD4^+$ cells (n) in the DLNs.

Results are representative of 2 independent experiments. Error bars represent means ± SD. CEC, controlled environment chamber. One-way ANOVA followed by Tukey's post hoc test was employed in the statistical analysis. Statistical significance levels are represented as *P < .05, **P < .01, ***P < .001, and ns, no significances.

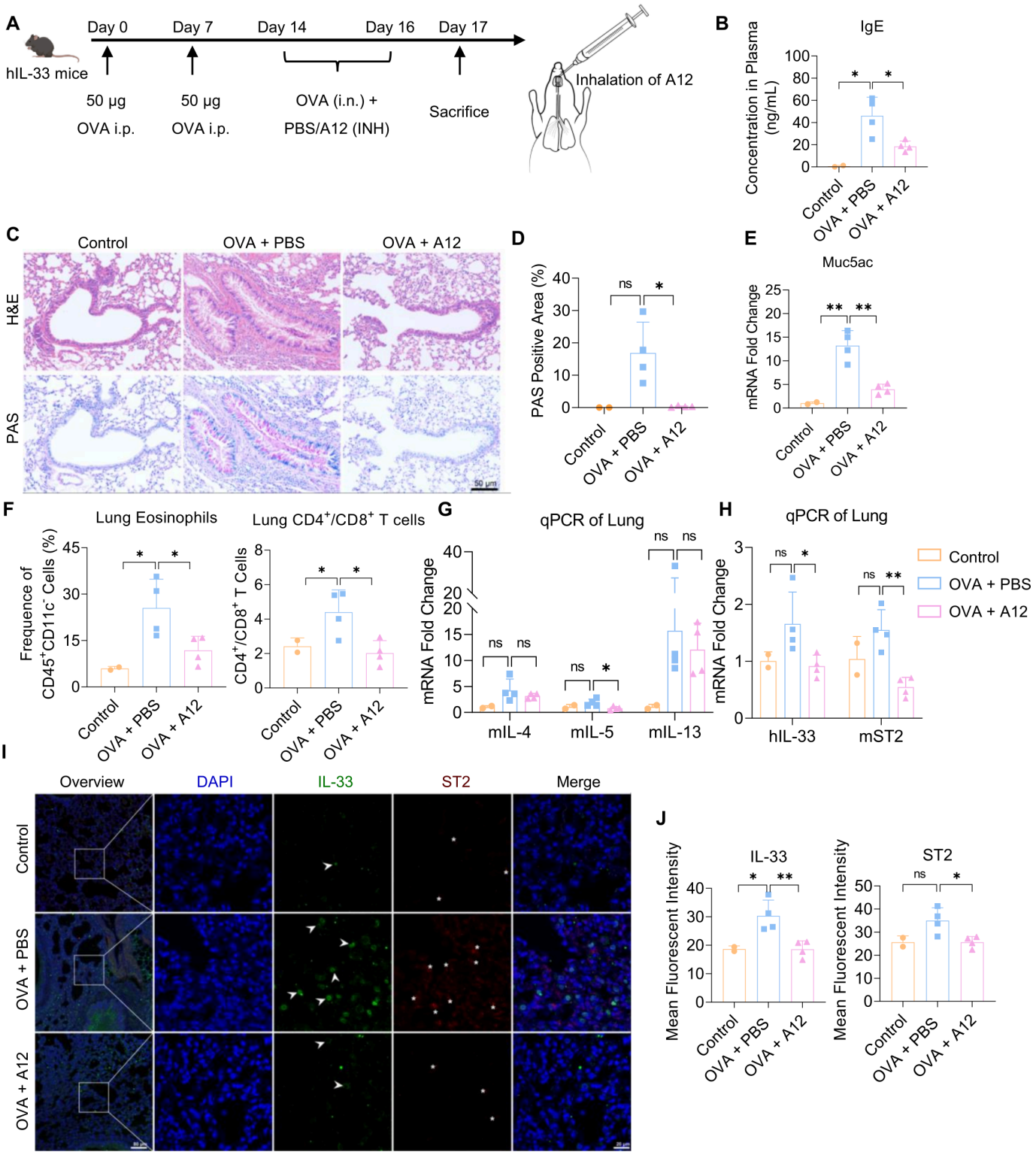

Figure 5

Inhalation of A12 suppresses OVA-induced experimental asthma.

A. Schematic diagram of therapeutic evaluation of A12 by inhalation in OVA-induced asthma in hIL-33 transgenic mice (n = 4). Naïve C57BL/6-IL-33$^{tm1(hIL-33)}$ mice were set as control (n = 2).

B. Serum IgE levels determined by ELISA.

C. H&E and Periodic acid–Schiff (PAS) lung section staining (original magnification x15). The scale bar is 50 µm.

D. Percentages of PAS positive area.

E. Expression of *Muc5ac* in lung tissue was measured by using RT-qPCR.

F. Lung immune cell quantification of mice exposed to OVA treated by PBS or A12 as indicated, as determined by using flow cytometry. Numbers on the representative fluorescence-activated cell sorting plots indicate the frequency of eosinophils and T cells.

G-H. Lung cytokine mRNA levels measured by RT-qPCR.

I-J. Immunofluorescence staining of hIL-33 and mST2 in lung (I) and mean fluorescent intensity (J).

Results are representative of 2 independent experiments. Error bars represent means ± SD. i.p., Intraperitoneal; INH, inhalation; i.n., Intranasal. One-way ANOVA followed by Tukey's post hoc test was employed to assess for multiple comparisons in the statistical analysis. Statistical significance levels are represented as *P < .05, **P < .01, ***P < .001, and ns, no significances.

Supplementary Files

This is a list of supplementary files associated with this preprint. Click to download.

- SupplementalinformationIL33.docx
- SupplementalfigureIL33CMI.pdf